EFFECTS OF LOADING RATE ON UNIAXIAL COMPRESSIVE STRENGTH OF SALT UNDER 273 TO 373 K

Suratwadee Sartkaew

A Thesis Submitted in Partial Fulfillment of the Requirements for the

Degree of Master of Engineering in Geotechnology

Suranaree University of Technology

Academic Year 2013

ผลกระทบของอัตราการให้แรงต่อกำลังกดในแกนเดียวของเกลือหิน ภายใต้อุณหภูมิ 273 ถึง 373 เคลวิน

นางสาวสุรัติวดี ศาสตร์แก้ว

วิทยานิพนธ์นี้เป็นส่วนหนึ่งของการศึกษาตามหลักสูตรปริญญาวิศวกรรมศาสตรมหาบัณฑิต
สาขาวิชาเทคโนโลยีธรณี
มหาวิทยาลัยเทคโนโลยีสุรนารี
ปีการศึกษา 2556

EFFECTS OF LOADING RATE ON UNIAXIAL COMPRESSIVE STRENGTH OF SALT UNDER 273 TO 373 K

Suranaree University of Technology has approved this thesis submitted in partial fulfillment of the requirements for a Master's Degree.

Thesis Examining Committee

_____

(Dr. Decho Phueakphum)

Chairperson

_____

(Prof. Dr. Kittitep Fuenkajorn)

Member (Thesis Advisor)

_____

(Dr. Prachya Tepnarong)

Member

_____ _____

(Prof. Dr. Sukit Limpijumnong) (Assoc. Prof. Flt. Lt. Dr. Kontorn Chamniprasart)

Vice Rector for Academic Affairs and Innovation

Dean of Institute of Engineering

สุรัติวดี ศาสตร์แก้ว : ผลกระทบของอัตราการให้แรงต่อกำลังกดในแกนเดียวของเกลือหินภายใต้อุณหภูมิ 273 ถึง 373 เคลวิน (EFFECTS OF LOADING RATE ON UNIAXIAL COMPRESSIVE STRENGTH OF SALT UNDER 273 TO 373 K) อาจารย์ที่ปรึกษา : ศาสตราจารย์ ดร.กิตติเทพ เฟื่องขจร, 74 หน้า.

วัตถุประสงค์ของงานวิจัยเพื่อศึกษาผลกระทบของอัตราการให้แรงต่อกำลังรับแรงกดและการเปลี่ยนแปลงรูปร่างของเกลือหินภายใต้อุณหภูมิสูง และเพื่อหาอัตราที่ปลอดภัยในการปล่อยอากาศออกจากโพรงเกลือที่ใช้กักเก็บอากาศอัด โดยอัตราการให้แรงในการทดสอบอยู่ระหว่าง 0.0001 ถึง 0.1 เมกกะปาสคาลต่อวินาที และทำการผันแปรอุณหภูมิจาก 273 ถึง 373 เคลวิน ผลการทดสอบระบุว่าค่าความเค้นและความเครียดภายใต้การผันแปรอัตราการให้แรงและอุณหภูมิมีลักษณะเป็นเส้นโค้งโดยเฉพาะอย่างยิ่งภายใต้อุณภูมิสูง ค่ากำลังรับแรงสูงสุดและค่าสัมประสิทธิ์ความยืดหยุ่นมีค่าเพิ่มขึ้นแบบลอการิทึมเมื่ออัตราการให้แรงเพิ่มขึ้นและมีค่าลดลงแบบเส้นตรงเมื่ออุณหภูมิเพิ่มขึ้น การรวมผลกระทบของความร้อนและอัตราการให้แรงเข้าไปในเกณฑ์การแตกดำเนินการโดยใช้พลังงานความเครียดเบี่ยงเบนของเกลือหินได้ถูกคำนวณในฟังก์ชั่นของพลังงานความเครียดเฉลี่ย แบบจำลองด้วยคอมพิวเตอร์ได้ถูกดำเนินการเพื่อหาค่าความเค้นและความเครียดรอบโพรงกักเก็บอากาศอัดภายใต้การผันแปรอัตราการลดลงของความดันภายในโพรง ค่าความเค้นและความเครียดสูงสุดขณะทำการปล่อยอากาศได้ถูกใช้ในการคำนวณค่าพลังงานความเครียดที่เกิดขึ้นบริเวณขอบเขตโพรง ผลการทดสอบได้ถูกเปรียบเทียบกับเกณฑ์การแตกที่ถูกพัฒนาขึ้นในข้างต้น และอัตราที่ปลอดภัยในการปล่อยอากาศออกจากโพรงกักเก็บอากาศอัดได้ถูกพิจารณาด้วย

สาขาวิชา เทคโนโลยีธรณี ลายมือชื่อนักศึกษา _____

ปีการศึกษา 2556 ลายมือชื่ออาจารย์ที่ปรึกษา _____

SURATWADEE SARTKAEW : EFFECTS OF LOADING RATE ON UNIAXIAL COMPRESSIVE STRENGTH OF SALT UNDER 273 TO 373 K. THESIS ADVISOR : PROF. KITTITEP FUENKAJORN, Ph.D., P.E., 74 PP.

THERMAL EFFECT/STRAIN ENERGY/COMPRESSION TEST/CREEP

The objective of this study is to determine effects of loading rate on compressive strength and deformability of the Maha Sarakham salt under elevated temperatures. The effort is aimed at determining the safe maximum withdrawal rates for the compressed-air energy storage (CAES) in salt caverns. The constant axial stress rates range from 0.0001 to 0.1 MPa/s. The testing temperatures are maintained constant between 273 and 373 Kelvin. The results indicate that the stress-strain curves monitored under various loading rates and temperatures show nonlinear relations, particularly under high temperatures. The salt strength and elasticity increase logarithmically with loading rate and decrease linearly with increasing temperature. To incorporate the thermal and rate (time-dependent) effects into a strength criterion the distortional strain energy at dilation of the salt is calculated as a function of the mean strain energy density. Finite difference analyses (FLAC 4.0) are also performed to determine the stresses and strains at the boundaries of CAES caverns for various reduction rates of the internal pressures. The maximum stresses and strains obtained during retrieval period are used to calculate the strain energy density induced at the cavern boundaries. The results are compared against the criteria developed above, and hence the safe maximum withdrawal rate of the compressed-air can be determined.

School of Geotechnology Student's Signature

Academic Year 2013 Advisor's Signature

ACKNOWLEDGMENTS

I wish to acknowledge the funding supported by Suranaree University of Technology (SUT).

I would like to express my sincere thanks to Prof. Dr. Kittitep Fuenkajorn for his valuable guidance and efficient supervision. I appreciate his strong support, encouragement, suggestions and comments during the research period. My heartiness thanks to Dr. Prachya Tepnarong and Dr. Decho Phueakphum for their constructive advice, valuable suggestions and comments on my research works as thesis committee members. Grateful thanks are given to all staffs of Geomechanics Research Unit, Institute of Engineering who supported my work.

Finally, I would like to thank beloved parents for their love, support and encouragement.

Suratwadee Sartkaew

TABLE OF CONTENTS

Page

TABLE OF CONTENTS (Continued)

Page

TABLE OF CONTENTS (Continued)

Page

LIST OF TABLES

Table **Page**

LIST OF FIGURES

Figure **Page**

LIST OF FIGURES (Continued)

Figure **Page**

LIST OF FIGURES (Continued)

Figure **Page**

LIST OF FIGURES (Continued)

Figure **Page**

LIST OF FIGURES (Continued)

Figure **Page**

SYMBOLS AND ABBREVIATIONS

$\partial\sigma_1/\partial t$	=	Loading rates
σ_1	=	Major principal stress
σ_2	=	Intermediate principal stress
σ_3	=	Minor principal stress
σ_C	=	Uniaxial compressive strengths
σ_m	=	Mean stress
ε_1	=	Major principal strains
ε_2	=	Intermediate principal strains
ε_3	=	Minor principal strains
ε_m	=	Mean strains
$\tau_{oct,f}$	=	Octahedral shear stresses at failure
$\gamma_{oct,f}$	=	Octahedral shear strains at failure
$\tau_{oct,d}$	=	Octahedral shear stresses at dilation
$\gamma_{oct,d}$	=	Octahedral shear strains at dilation
E, E_1	=	Elastic modulus
E_2	=	Spring constant in visco-elastic phase
η_1	=	visco-plastic coefficient in steady-state phase
η_2	=	visco-elastic coefficient in transient phase
ν	=	Poisson's ratio

SYMBOLS AND ABBREVIATIONS (Continued)

G	=	Shear modulus
ε_c	=	Total compressive strain
ε_c^e	=	Elastic strain
ε_c^c	=	Plastic creep strain
$\partial\tau_{oct}/\partial t$	=	Octahedral shear stress rate
W_d	=	Distortional strain energy
W_m	=	Mean strain energy
T	=	Absolute temperature
t	=	Time
α	=	Stress constant
β	=	Stress exponent
κ	=	Time exponent
λ	=	Temperature constant
ψ	=	Empirical constant related to G and T
χ	=	Empirical constant for equation (5.1)
ξ	=	Empirical constant for equation (5.1)
ξ	=	Empirical constant for equation (5.1)
ℓ	=	Empirical constant for equation (5.1)
δ	=	Empirical constant for equation (5.10)
ω	=	Empirical constant for equation (5.10)
ς	=	Empirical constant for equation (5.10)

SYMBOLS AND ABBREVIATIONS (Continued)

ɘ	=	Empirical constant for equation (5.15)
η	=	Empirical constant for equation (5.15)
ι	=	Empirical constant for equation (5.15)
ɘ′	=	Empirical constant for equation (5.16)
η′	=	Empirical constant for equation (5.16)
ι′	=	Empirical constant for equation (5.16)
ϖ	=	Empirical constant for equation (5.17)
ϑ	=	Empirical constant for equation (5.17)
ζ	=	Empirical constant for equation (5.17)
φ	=	Empirical constant for equation (5.17)
ϖ′	=	Empirical constant for equation (5.18)
ϑ′	=	Empirical constant for equation (5.18)
ζ′	=	Empirical constant for equation (5.18)
φ′	=	Empirical constant for equation (5.18)

CHAPTER I

INTRODUCTION

1.1 Background and rationale

The effects of loading rate on the compressive strength and deformability of intact rocks have long been recognized (Kumar, 1968; Jaeger et al., 2007; Cristescu and Hunsche, 1998; Albertin et al., 1999). For rock salt such effects have been studied by various researchers (Fuenkajorn et al., 2012; Liang et al., 2011; Lajtai et al., 1991; Hamami, 1999). It has been found that the salt strength increases with the applied stress and strain rates. The rock strength and elastic properties have been known to decrease as the temperature increases (Sriapai et al., 2012). Several formulations have been proposed to describe the temperature-dependent behavior of rock salt (Sriapai et al., 2012; Sheinin and Blokhin, 2012). Such knowledge is necessary for stability analysis and design of the salt storage caverns. During injection period the storage caverns may subject to temperatures as high as 140°C (414 K), depending on the injection rate and the maximum storage volume and pressure. The effects of loading rate under elevated temperatures of rock salt have however rarely been investigated.

1.2 Research objectives

The objectives of this study are to experimentally assess the influence of loading rate on the compressive strength and deformability of rock salt under

constant temperatures of 273, 303, 343 and 373 Kelvin. This selected range of temperatures covers those likely occur around salt storage caverns under operation. Uniaxial compression test have been performed on the Maha Sarakham salt under loading rates of 0.0001, 0.001, 0.01 and 0.1 MPa/s. The strain energy density criteria are proposed to describe the salt strength as affected by the loading rates and temperatures. Computer simulations are determining the safe maximum withdrawal rates for the compressed-air energy storage (CAES) in salt caverns.

1.3 Research methodology

The research methodology shown in Figure 1.1 comprises 7 steps; including literature review, sample preparation, laboratory testing, calibration of elastic and creep parameters, development of strength criteria, computer simulations, discussions, conclusions and thesis writing.

1.3.1 Literature review

Literature review is carried out to study the previous researches on time-dependent behavior of rock salt as affected by mechanical and thermal loadings. The sources of information are from text books, journals, technical reports and conference papers. A summary of the literature review is given in chapter two.

1.3.2 Sample preparation

The salt specimens are prepared from 47 mm salt cores drilled from depths ranging between 270 and 330 m by Siam Submanee Co., Ltd. in the northeast of Thailand. The salt cores belong to the Lower Salt member of the Maha Sarakham formation. Tabakh et al. (1999) describe the origin and geologic sequence of the Maha Sarakham salt. The drill cores were dry-cut to obtain cylindrical shaped

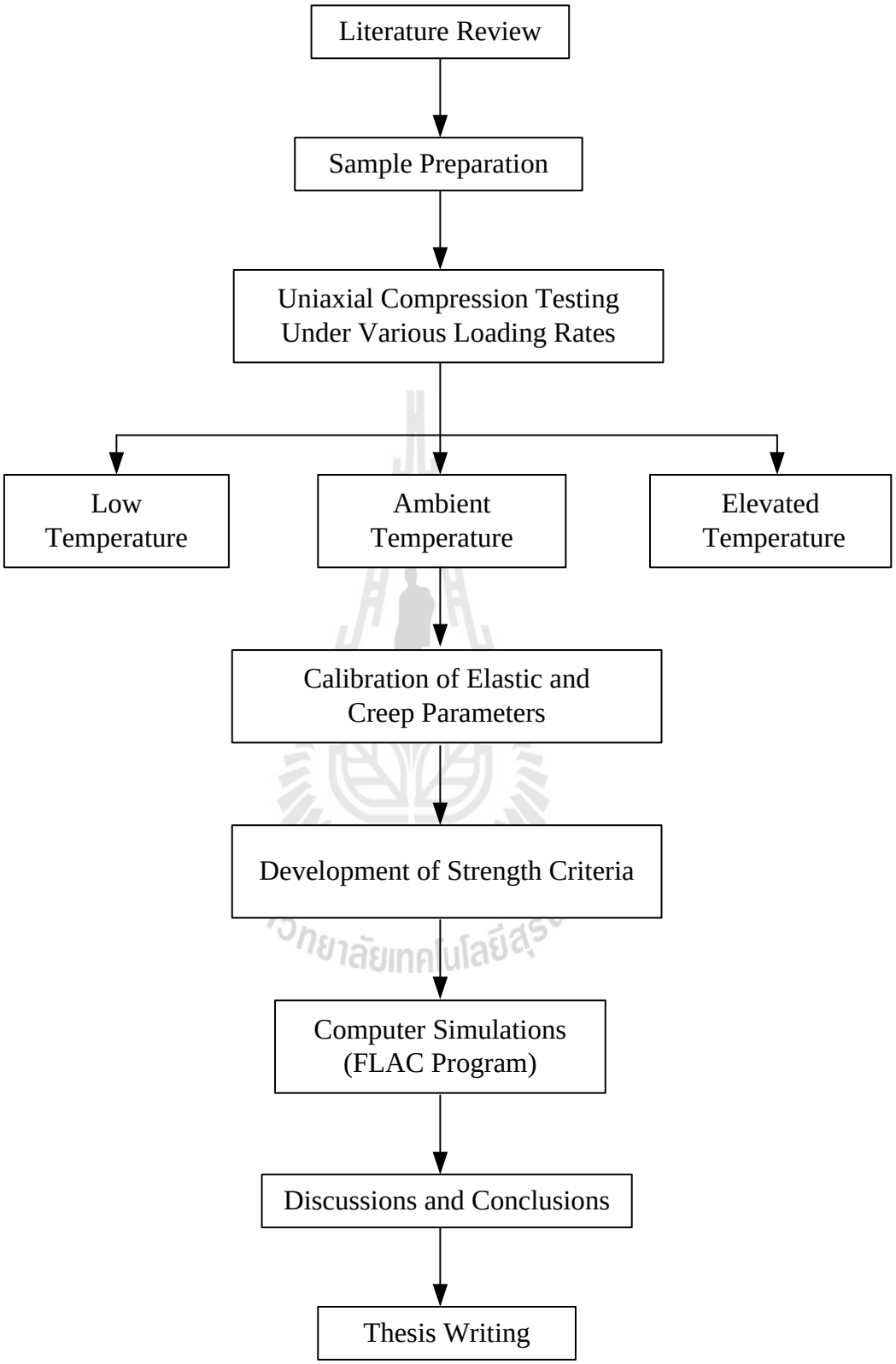

Figure 1.1 Research methodology.

specimens with nominal dimensions of 47 mm diameter and 118 mm length.

1.3.3 Laboratory testing

The uniaxial compression tests have been performed to determine the time-dependent properties of the Maha Sarakham salt under controlled loading rates from 0.0001 to 0.1 MPa/s. The testing temperatures range from 273 to 373 Kelvin. The electronic load cell is used to record loading increasing. The load at failure is recorded to calculate the salt compressive strength. The specimen deformations are monitored with four dial gages to calculate the compressive strains. Photographs are taken of the failed specimens.

1.3.4 Calibration of elastic and creep parameters

The results are used to determine the elastic and transient creep parameters. The regression analysis on the tests data using SPSS statistical software (Wendai, 2000) is performed to determine the elastic and creep parameters.

1.3.5 Development of strength criteria

Results from laboratory measurements in terms of the octahedral shear strength of rock salt are used to formulate mathematical relations. Various formulations of loading rate and temperature dependent strength and deformability are derived. To incorporate the thermal and rate (time-dependent) effects into strength criteria the distortional strain energy at dilation and failure of the salt is calculated as a function of the mean strain energy density.

1.3.6 Computer simulations

The finite difference program – FLAC (Itasca, 1992) are used to determine the stresses and strains at the boundaries of CAES caverns for various reduction rates of the internal pressures. The principal stresses and strains under

various air withdrawal rates are calculated and compared against the strength criteria.

1.3.7 Discussions, conclusions and thesis writing

The results of testing and modeling are discussed to reveal the scope and limitation of their applications. All research activities, methods, and results are documented and complied in the thesis. The research or findings are published in the conference proceedings or journals.

1.4 Scope and limitations

The scope and limitations of the research include as follows.

1. All tests are conducted on rock salt specimens obtained from the Lower Salt member of the Maha Sarakham formation in northeastern Thailand.
2. The applied loading rates vary from 0.0001, 0.001, 0.01 to 0.1 MPa/s.
3. The testing temperatures range from 273 to 373 Kelvin.
4. Testing is made under dry condition.
5. Up to 30 samples are tested.
6. The nominal dimensions of cylindrical shaped specimens with 47 mm diameter and 118 mm length.
7. Finite difference analyses (FLAC 4.0) are also performed to determine the stresses and strains at the boundaries of CAES caverns for various reduction rates of the internal pressures.
8. The research findings are published in conference paper or journal.

1.5 Thesis contents

Chapter I describes the objectives, the problems and rationale, and the methodology of the research. Chapter II present results of the literature review on temperature and loading rate effects on salt, temperature and loading rate effects on other rocks and constitutive models with incorporating temperature effects. Chapter III describes the salt sample collection and preparation. Chapter IV describes the laboratory testing and test results. Chapter V describes the compressive creep strain and strength criteria. Chapter VI describes the computer simulations are also performed to determine the stresses and strains at the boundaries of CAES caverns. Chapter VII summarizes the research results, and provides recommendations for future research studies.

CHAPTER II

LITERATURE REVIEW

2.1 Introduction

The topics reviewed here include temperature and loading rate effects on salt, temperature and loading rate effects on other rocks and constitutive models with incorporating temperature effects.

2.2 Temperature effect on salt mechanical properties

Charpentier (1984) proposes the time-dependent behavior of rock salt under temperature has guided the "Laboratorie de Mecanique des Solides" to develop specific creep equipment. The design and capacity of this creep test installation offer the possibility of studying a wide range of materials. Considering the characteristics of the problem the "Laboratorie de Mecanique des Solides" has designed a specific creep equipment to carry out long term at high temperature. At present, the experimental installation of three temperature levels between 20°C and 200°C for uniaxial creep. The specimens used are cylinders of 7 cm in diameter and 16 cm in height on Bresse salt. Two specimens test at 20°C applies the uniaxial stresses of 15.3 MPa and 17.8 MPa correspond respectively to 65% and 75% of the uniaxial compressive strength. The creep was observed during two months. At this stage the strain rate is not stable yet and they are still in a transient phase for the two samples. This primary creep can be interpreted by means of a time-hardening law. Test at 10

0°C applies the uniaxial stresses of 11.3 MPa and 15.3 MPa correspond respectively to 65% and 75% of the uniaxial compressive strength. During about 30 days the values of $\dot{\varepsilon}$ are 13×10^{-6} hr^{-1} and 18×10^{-6} hr^{-1}. For the most severely loaded sample, the increase of the strain rate after two months denotes the existence of a tertiary state which can probably lead to failure. Three specimens obtained on test at 200°C. The uniaxial stresses of 3.4 MPa, 5 MPa and 7.5 MPa correspond respectively to 20%, 30% and 45% of the uniaxial compressive strength. For the two specimens with the highest levels of load the creep is very important, the strains are 15% and 25% after about two months. This fact shows the major effect of temperature on the time-dependent behavior of rock salt. For the specimens with the smallest load, they have measured only 2% of strain after two months. This difference leads us to consider a yielding point for the behavior law of our rock salt.

Hansen (1984) studies the physical and mechanical variability of natural rock salt for four experimentally deformed rock salts in the United States. The influence on creep deformation of impurity content decreases as temperature increases. The rate controlling deformation mechanism shows similar stress and temperature dependency for each salt, being independent of purity. Dislocation glide dominates the deformation at low temperature, i.e. 25°C; whereas at high temperature, i.e. 200°C dislocation climb is the predominant mechanism.

Hamami et al. (1996) study the effect of temperature and conclude that the temperature increase, as for the deviatoric stress, results in an increase of the material deformation. Cristescu and Hunsche (1996) study the temperature effect on the strain rate suitable for laboratory testing. They suggest that the appropriate strain rate for

testing at 100 °C and 200 °C is 10^{-8} s^{-1} and 10^{-7} s^{-1} because the temperature can affect the creep deformation and strength of salt under high temperatures.

Temperature or heating affects the creep deformation, because they increase the plastic property of salt and long-term deformation (Pudewills, 1995). Jeremic (1994) postulates that rock salts lose their brittleness after extension tempering at approximately 600 °C and exhibit a critical shear stress up to 1 MPa.

Sheinin and Blokhin (2012) study the thermomechanical effects in rock salt samples under uniaxial compression for identifying the deformation processes in geomaterials under the wider range of condition, namely, under the stresses coming to the elastic and ultimate strengths, by measuring the thermal radiation. Two following groups of cylindrical samples from two different deposits were prepared in the stress range $\sigma_e < \sigma_1 < \sigma_c$.

1) at constant loading rate ($d\sigma_1/ dt$) from 0.05 to 0.5 MPa/s.
2) at constant rate of change of the longitudinal strain ($d\varepsilon_1/ dt$) from 0.005 to 0.02 mm/s.

Figure 2.1 shows the IR radiation intensity and $V_m(\sigma_1)$, which were obtained under loading rates of 0.2 and 0.1 MPa/s, contain the horizontal portion in the elastic deformation domain, where the heat exchange with the environment hinders establishment of the change in temperature of the sample due to thermo mechanical processes.

The relationships $V_m(\sigma_1)$ at $d\varepsilon_1/dt$ = constant and $d\sigma_1/dt$ = constant, wherein the guasiadiabaticity condition is fulfilled as well (curves 1 and 2 in Figure 2.1), are similar. Therefore, the inflection point in the plot $V_m(\sigma_1)$ at $\sigma_1 \approx 22$ MPa can be taken

as the elastic limit for the given sample. The analysis of the curve σ_1 - ε_1 proves this fact (Figure 2.2).

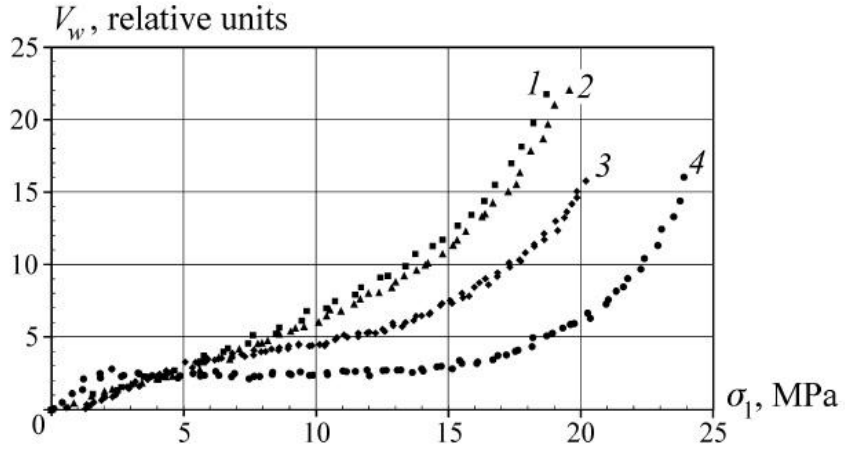

Figure 2.1 The relationships between the IR radiation intensity and the longitudinal stress $V_m(\sigma_1)$ at different loading rates $d\sigma_1/dt$: 1-0.5; 2-0.35; 3-0.2; 4-0.1 MPa/s (Sheinin and Blokhin, 2012).

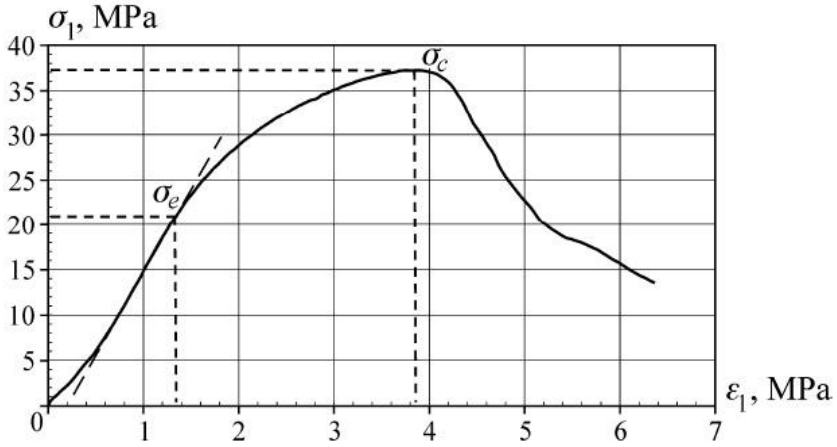

Figure 2.2 The curve σ_1 - ε_1 at $d\varepsilon_1/dt$ = 0.01 mm/s (Sheinin and Blokhin, 2012).

Sriapai et al. (2012) study the temperature effects on salt strength by incorporating empirical relations between the elastic parameters and temperatures of the tested specimens to describe the distortional strain energy density of rock salt under different temperatures and deviation stresses. The results are obtained under temperatures ranging from 273 to 467 Kelvin. The results indicate that the uniaxial compressive strengths (σ_c) of salt decrease linearly with increasing temperature. The tensile strength (σ_B) also decreases linearly with increasing specimen temperature (Figure 2.3).

Khathipphathee and Fuenkajorn (2013) proposed performance assessment of the Maha Sarakham salt for CO_2 storage. The testing temperatures are 273 and 303 Kelvin. The tests methods and calculation follow the ASTM (D7070-08) standard practices. The test duration is 21 days. The exponential creep law is used to describe the time-dependent deformations of the salt specimens. The test results indicate that the creep deformation increases with the temperatures. The test results show that the transient creep under low temperature decreases with time and tends to be constant at steady-state creep phase. Temperature exerts an effect on deformability and strength of rocks (Vosteen and Schellschmidt, 2003; Shimada and Liu, 2000; Okatov et al., 2003). It has been found that rock strength and elastic properties decrease as the temperature increases.

2.3 Loading rate effect on Salt

Lajtai et al. (1991) study the effect of strain rate on strength on two widely different rock types. Tyndallstone is a brittle material that deforms in an approximately elastic manner. The second rock Lanigan potash, is a ductile salt rock

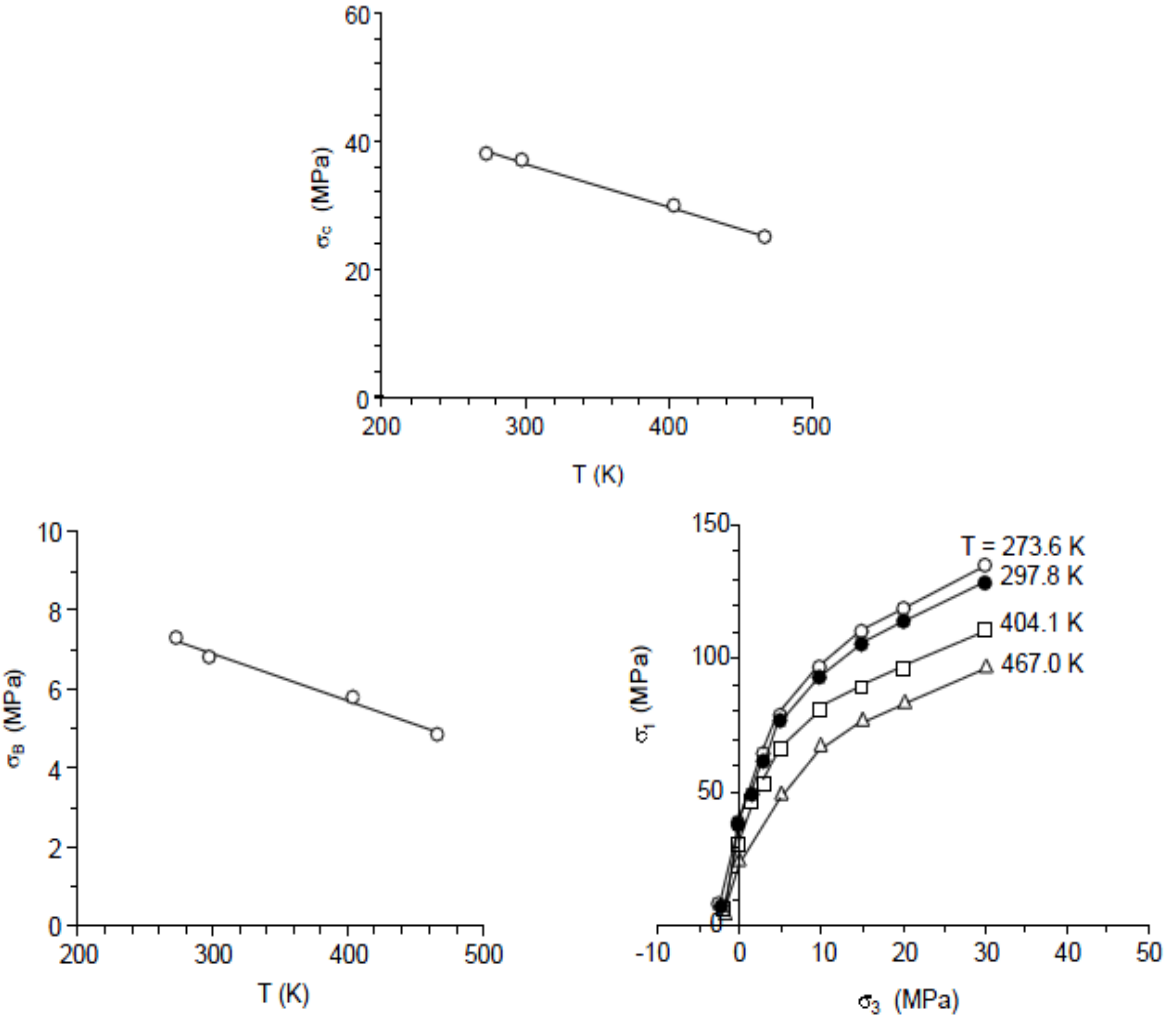

Figure 2.3 (a) Uniaxial compressive strength of salt as a function of temperature.

(b) Brazilian tensile strength of salt as a function of temperature.

(c) Major principal stress at failure as a function of confining pressure.

that has a strongly nonlinear stress-strain curve. Lanigan potash is test five uniaxial compression, three confining at 2 and 5 MPa. In uniaxial compression, five different strain rates were used: 0.035, 0.11, 1.75, 3 and 25 μ ε /s. For the triaxial tests, only three rates: 0.11, 1.75 and 25 μ ε /s were employed. Figure 2.4 shows the Langian

data for both uniaxial and triaxial conditions when the appropriate curve-fitting constant A and B are used the logarithmic function:

$$Y = A + B\ln(X) \tag{2.1}$$

where A and B are constants.

The strain rate effect for Lanigan potash rock rock are using the Rocker function for Lanigan potash, the general criterion of strength becomes:

$$\sigma_{1fn}(p,v) = \left(1 - \frac{p}{T_0}\right)^{R_0} + \frac{1}{C_0}\left[(B_0 - D) + D\left(1 - \frac{|p|}{T_0}\right)^{R_0}\right]^{R} \ln\left(\frac{v}{v_0}\right) \tag{2.2}$$

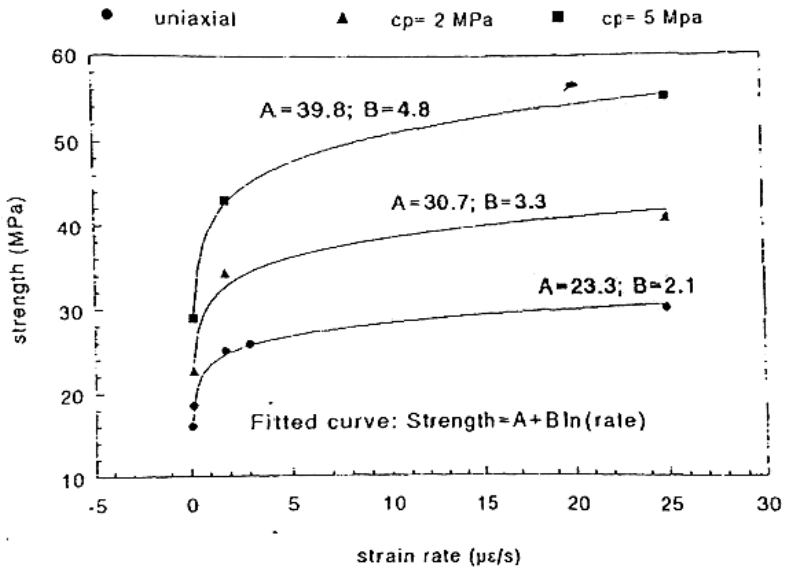

Figure 2.4 Dynamic strength tests on Lanigan Potash rock. (Lajtai et al., 1991).

A subscript is attached is to the exponent R to signify that the Rocker function was fitted to the data conducted at the standard rate of 25 με/s. For Lanigan potash, the appropriate strength parameters and fitting constants for Equation (2.2), at the standard rate are:

$$T_0 = -2 \text{ MPa}, C_0 = 3 \text{ MPa}, R_0 = 0.49, B_0 = 2.1 \text{ and } D = 3.7 \quad (2.3)$$

Using above parameters Equation (2.2) was fitted to the triaxial data for Lanigan potash rock (Figure 2.5). The data for three rates are shown with the best fit curve. No triaxial tests were completed at the slowest rate; the broken line follows the prediction according to Equation (2.2). The effect of the strain rate is quite large, with the slower rates causing a considerable reduction in standard triaxial strength. The data available suggest that the rate effect becomes greater with increasing confining pressure.

Dubey and Gairola (2005) study the stress-strain behavior and mechanics properties on rock salt samples collected from Guma rocksalt Mine, India. Cylindrical samples cored perpendicular to the bedding planes, were compressed using an automated closed loo[servo-controlled testing machine at stress rates ranging from 9.12×10^{-3} MPa/minute to 9.12 MPa/minute. The stress-strain curves obtained by compression of rocksalt specimen at various stress rate exhibit similar pattern but there are distinct differences in geometry (Figure 2.6).

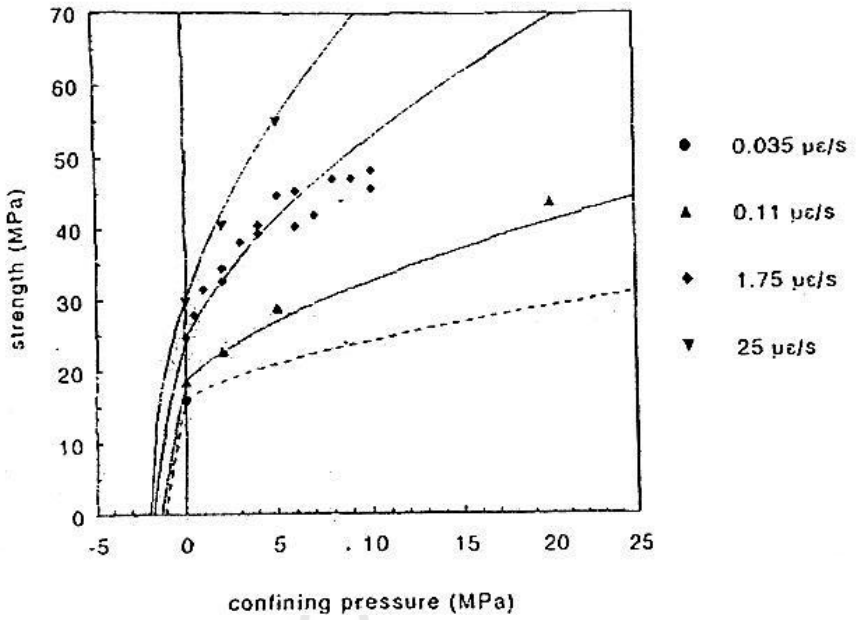

Figure 2.5 Compressive strength of Lanigan potash at various loading rate (Lajtai et al., 1991).

The stress-strain curves reveal that at low stress rates rocksalt exhibits plastic deformation and at high stress rates it exhibits more brittle deformation.

It is considered that the modulus of elasticity is independent of the stress rate. However, the non-linear nature of the stress-strain curve up to the yield point at low stress rates in the present experiments, reveals that the modulus is stress rate dependent (Figure 2.7).

The ratio of compaction stresses (σ_c) to yield stresses (σ_y) decreases whereas the ratio of yield stress (σ_y) to peak stress (σ_p) increases with the progressive increase in stress rates of deformation (Figure 2.8).

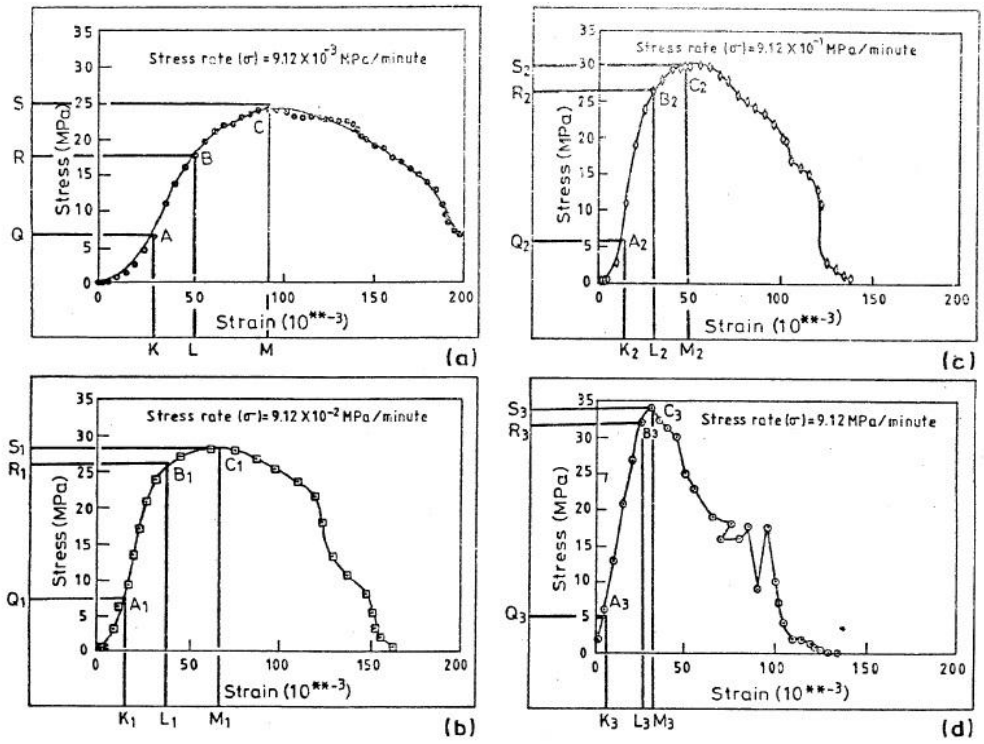

Figure 2.6 Stress-strain behavior at stress rate (a) 9.12 $\times 10^{-3}$ MPa/minute (b) 9.12 $\times 10^{-2}$ MPa/minute (c) 9.12 $\times 10^{-1}$ MPa/minute (d) 9.12 MPa/minute of deformation of rocksalt from Guma, District Mandi, H.P., India (Dubey and Gairola, 2005).

The mechanical properties like yield stress, peak stress, compaction stress, compaction strain and failure strain in rock salt undergoing deformation by compression are stress rate dependent. The present work suggests that at very high stress rates the yield stress and peak stress could become equal and at high stress rates rock salt exhibits brittle deformation. For the lower stress rates, the peak stress is not equal to the yield stress and the rock salt deforms by viscoplastic flow. As the stress

rates decrease the peak stress and yield stress decreases and compaction stress and the compaction strain increases.

Liang et al. (2011) study the strain rate effect on mechanics properties of salt rock by uniaxial compression test under loading with $\dot{\varepsilon}$ value of $2x10^{-5}$, $2x10^{-4}$ and $2x10^{-3}$/s. Average UCS values are 13.6, 13.9, and 12.4 MPa, respectively for $\dot{\varepsilon}$ values of $2x10^{-5}$, $2x10^{-4}$ and $2x10^{-3}$/s. From the result of uniaxial compression test with different strain rate it found that the peak strength of rock salt is little affected by the strain rate (within the chosen range for $\dot{\varepsilon}$). The relationship between strain rate and strain failure of rock salt: with increasing $\dot{\varepsilon}$ value, the strain at peak strength is less. For example, the strain-to- failure is 1.3-1.7% (specimen #1, #2) when $\dot{\varepsilon}$ = $2x10^{-5}$/s; however, it decrease to 0.3-0.7% (specimen #5,#6) when $\dot{\varepsilon}$ is increased to $2x10^{-3}$/s as shown in Figure 2.9.

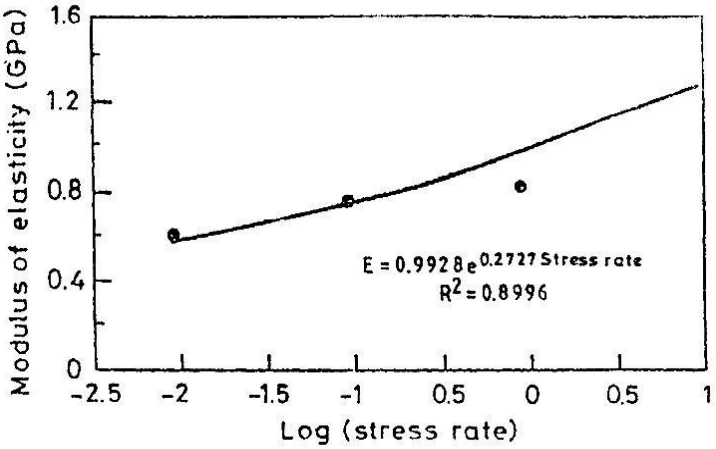

Figure 2.7 Variation of modulus of elasticity with stress rate of deformation of rock salt from Guma, District Mandi, H.P., India (Dubey and Gairola, 2005).

The rock strength of salt rock is only slightly affected by loading strain rate. The elastic modulus slightly increases with strain rate, but the increment is small. Under the same strain rate, the strength of thenardite is somewhat larger than rock salt, mainly related to crystal grain size and fabric of the minerals.

Fuenkajorn et al. (2012) study the effects of loading rate on strength and deformability of the Maha Sarakham salt under ambient temperature. The uniaxial and triaxial compression tests have been performed to assess the influence of loading rate on the compressive strength and deformability of the Maha Sarakham salt. The lateral confining pressures are maintained constant at 0, 3, 7, 12, 20 and 28 MPa while the axial stresses are increased at constant rates of 0.001, 0.01, 0.1, 1.0 and 10 MPa/s. until failure occurs. It was also found that the salt elasticity and strength increase with the loading rates, as shown in Figure 2.10. The elastic (tangent) modulus determined

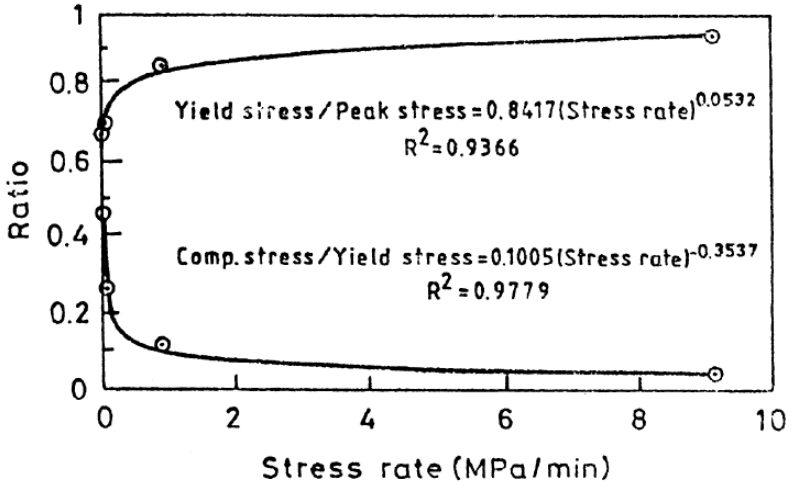

Figure 2.8 Variation of ratio of compaction stress/yield stress and yield stress/peak stress with stress rate of deformation of rock salt from Guma, District Mandi, H.P., India (Dubey and Gairola, 2005).

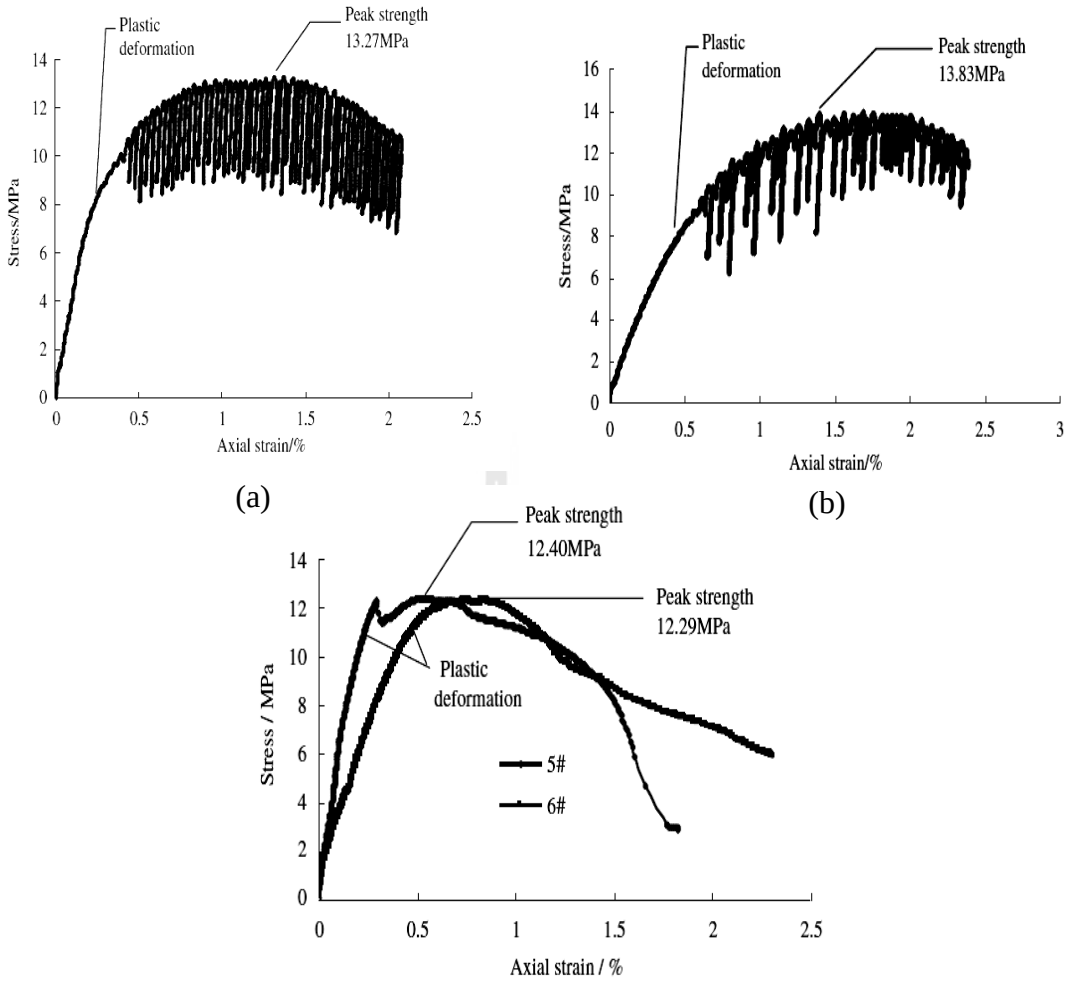

Figure 2.9 (a) Stress-strain curve of halite with strain rate of $2.0x10^{-5}$/s (specimen#1).

(b) Stress-strain curve of halite with strain rate of $2.0x10^{-5}$/s (specimen#2).

(c) Stress-strain curve of halite with strain rate of $2.0x10^{3}$/s (specimen#5, #6). (Liang et al., 2011)

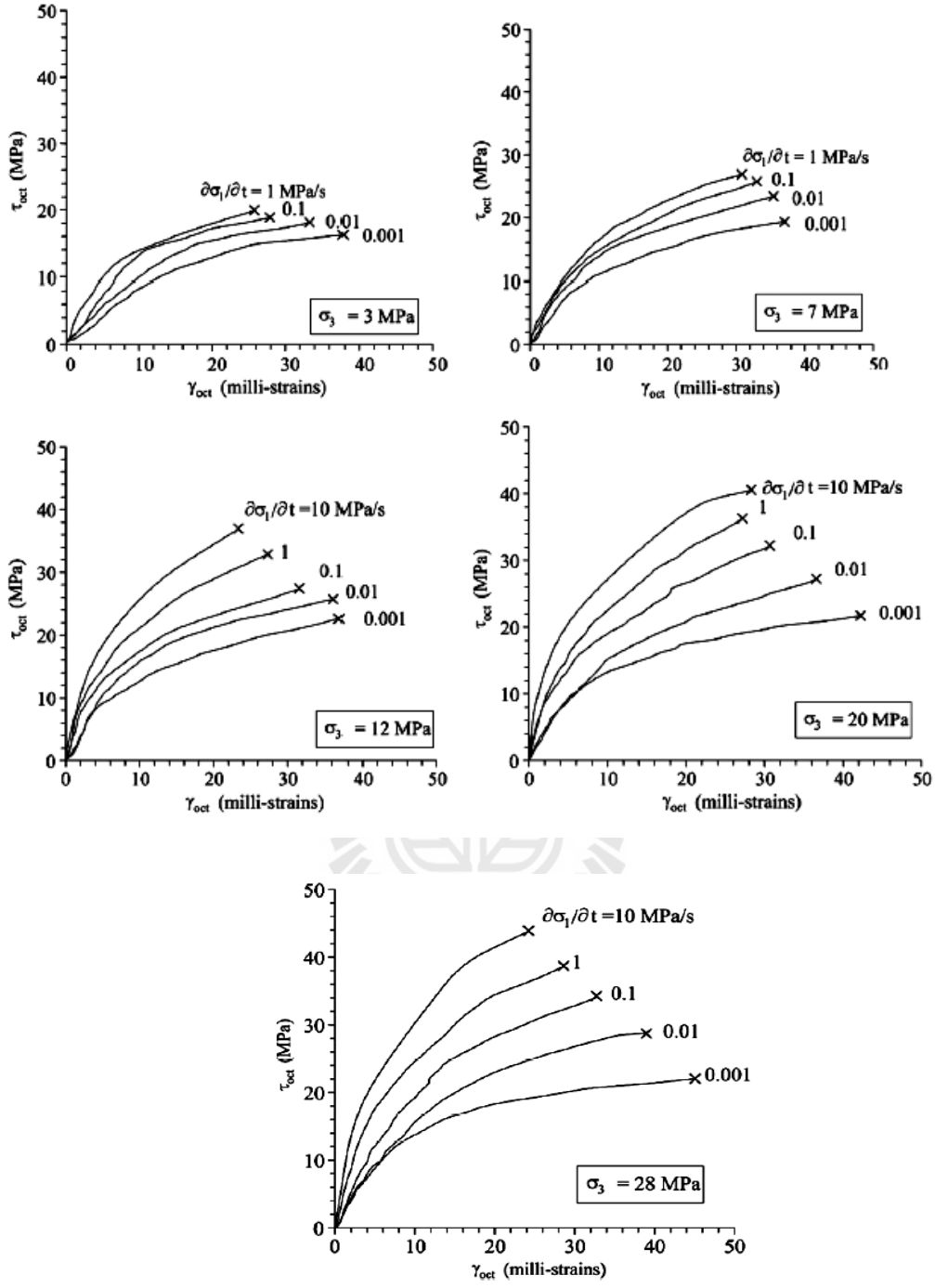

Figure 2.10 Octahedral shear stress (τ_{oct}) as a function of octahedral shear strain (γ_{oct}) for various confining pressures (σ_3) and loading rates ($\partial\sigma_1/\partial t$) (Fuenkajorn et al., 2012).

at about 40% of the failure stress varies from 15 to 25 GPa, and the Poisson's ratio from 0.23 to 0.43. The elastic parameters tend to be independent of the confining pressures. The strains induced at failure decrease as the loading rate increases.

2.4 Temperature consideration in constitutive modeling

Langer (1984) and Farmer (1983) present numerous empirical equations describing the time - dependent behavior of geological materials. Two types of empirical laws that explicitly contain creep strain, stress, and time variables are selected for use this investigation potential laws and exponential laws. The laws are applied to describe salt behavior without considering the actual mechanism of deformation. Generally, empirical constitutive models are developed by linking the creep strain to stress and temperature. The potential laws are power equations relating creep strain, stress, time and temperature. Two empirical models describing transient and steady – state creep strains can be expressed as:

$$\varepsilon(t) = K'\sigma^{\beta} t^{\gamma} T^{\alpha} \quad \text{(transient)} \tag{2.4}$$

$$\dot{\varepsilon}(t) = A'\sigma^{B} T^{C} \quad \text{(steady – state)} \tag{2.5}$$

The exponential laws present the transient creep strain as a function of stress, time and temperature in exponential form:

$$\varepsilon(t) = B'\sigma^{m} t^{n} \exp(-\lambda / T) \tag{2.6}$$

where $\varepsilon(t)$ is transient creep strain, $\dot{\varepsilon}(t)$ is steady – state creep strain rate, σ is stress, t is time, T is absolute temperature, K′, α, β, γ, A′, B, C, B′, m, n, λ is empirical constants.

Pudewills and Droste (2003) study the numerical simulation of the thermal and thermomechanical response of the large-scale in situ experiment ‘‘thermal simulation of drift emplacement’’, which was carried out in the Asse salt mine in Germany. The analyses concern the modeling of the temperature fields, thermally induced drift closure followed by the consolidation of backfill material and the distribution of the stresses. Finite element codes (ADINA and MAUS) specially developed for the repository structures as well as a general-purpose code have been used. The primary objective of the investigations is to evaluate the capability of these codes to simulate the thermomechanical behavior of rock salt and backfill material under representative conditions of a waste repository by comparing of calculated results with in situ measurements. An overall good agreement between modeling and in situ measured results indicates that most thermomechanical effects are fairly well represented by the numerical models.

The thermomechanical behavior of rock salt is described in the finite element analyses by a thermoelastic material model with a temperature-dependent steady-state creep and based on the experimental results. According to this model, the total strain rate is given as the sum of elastic, thermal, and steady-state creep rates. This constitutive relation governing the creep strain rate of rock salt is described as follows:

$$\varepsilon_{ef} = A\sigma^{5}_{ef} \exp(-Q/(RT)) \quad (2.7)$$

Yanan et al. (2010) propose the constitutive models of rock as affected by temperature and humidity. Based on the Nishihara model, a visco-elastic-plastic rock model was established by using the coefficients of thermal and humidity expansion, thermal viscosity attenuation, humid viscosity attenuation and acceleration rheology components. They used the definition of a controlled heat circle to explain the model. The results show that the behavior of rock, affected by temperature and humidity, is stable as a function of time when the stress is lower than the first yield stress (σ_{S1}). The creep rate will increase due to the effect of temperature and humidity when the stress is greater than or equal to the first yield stress (σ_{S1}), the creep rate will accelerate at an increasing rate when the stress is greater than or equal to the second yield stress (σ_{S2}) shown in Figure 2.11.

In Figure 2.11, E_1, E_2 are the stiffness coefficients of springs, α_1, α_2 are the thermal expanding coefficients of springs, β_1, β_2 are the humidity expanding coefficients of springs and β_{22}, β_3, β_4 the humidity attenuation coefficients of dashpots. η_1, η_2, η_3 are viscosity parameters and ξ_1, ξ_2, ξ_3 the temperature attenuation coefficients of dashpots. σ_{S1} is the first yield stress which is the threshold value of the increasing creep rate and σ_{S2} is the second yield stress, i.e., the threshold value of accelerated creep. T, W are temperature and humidity respectively.

If $\sigma < \sigma_{S1}$, the model is composed of a spring and a Kelvin element, hence:

$\varepsilon = \varepsilon_1 + \varepsilon_2, \varepsilon \xrightarrow{t\to\infty} 0$, the creep deformation of the wall rock will be stable. If $\sigma_{S1} \leq \sigma < \sigma_{S2}$, the model is composed of a spring, a Kelvin element and an ideal visco –

plastic element, hence: $\varepsilon = \varepsilon_1 + \varepsilon_2 + \varepsilon_3, \dot{\varepsilon} \xrightarrow{t\to\infty} \beta_3 W + \xi_2 T + \frac{\sigma_0 - \sigma_{S1}}{\eta_2}$, the rate of the wall rock will increase remain constant at a constant value. If $\sigma \geq \sigma_{S2}$, the model is composed of a spring, a Kelvin element and an ideal visco-plastic element and an acceleration rheology component, $\varepsilon \xrightarrow{t\to\infty} \beta_3 W + \xi_2 T + \frac{\sigma_0 + \sigma_{S1}}{\eta 2} t$, the creep rate will accelerate at a constant rate and failure will occur,which results in a failure of the roadway. The model derived in this study can completely describe visco - elastic-plastic characteristics and can reflect the three stages of rock creep.

2.5 Temperature effect on other rocks

Kumar (1968) studies the effect of stress rate and temperature on the strength of basalt and granite. The ultimate strengths of basalt and granite were measured over a range of stress rates from 2×10 to 3×10^{10} psi per second. A comparison of basalt and granite showed that, although their static strength was close (Figure 2.12),

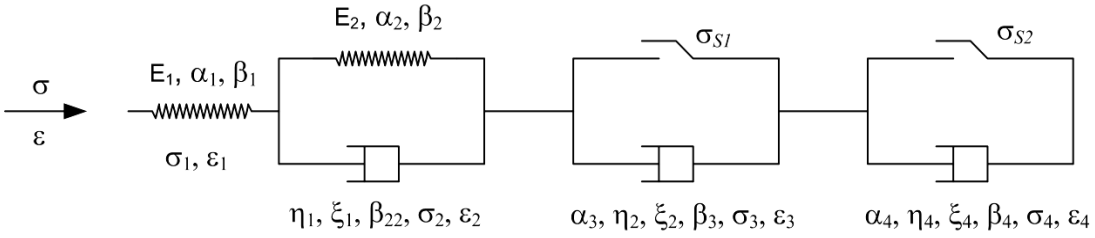

Figure 2.11 Visco-elastic-plastic constitutive models with temperature-humidity effects (Yanan et al., 2010).

their dynamic strengths were different. The static strengths of basalt and granite were 27.5 and 29 kpsi respectively at the stress rate of 2×10 psi per second while their strengths at the stress rate of 3×10^{10} psi per second were 59 and 70 kpsi respectively. In order to obtain an insight into the basic mechanisms of rock fracturing, the combined effects of stress rate and temperature were studied. The strength of basalt was increased from 27.5 kpsi at room temperature to 45 kpsi at liquid nitrogen temperature at the stress rate of 2×10 psi per second. The mechanisms of fracturing were thermally activated. The activation energy for basalt at 50 kpsi equaled 450 calories per mole. The effect on the strength of increasing the

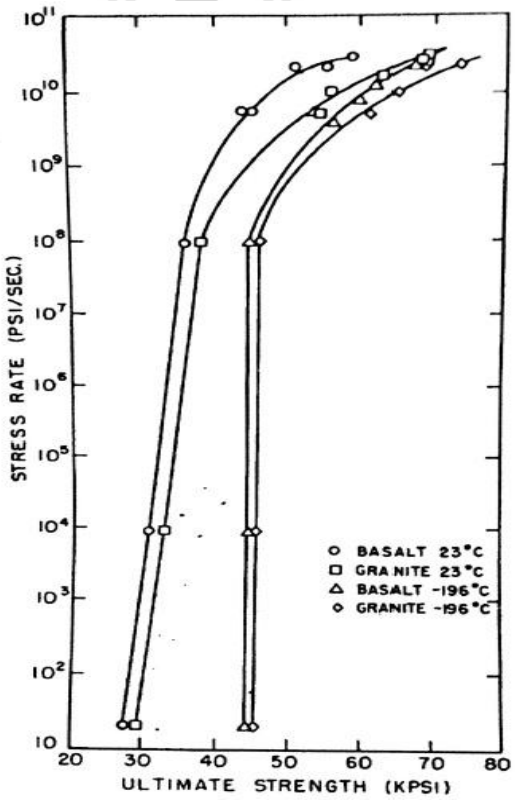

Figure 2.12 Effect of stress rate on the fracture strength of basalt and granite at various temperatures (Kumar, 1968).

stress rate was similar to the effect produced by lowering the temperature as shown in Figures 2.13 and 2.14.

Yang and Daemen (1997) investigate the temperature effects on creep of tuff. Creep tests have been conducted at room temperature and at elevated temperature (204 °C). In order to model the creep behavior of tuff, a new time-dependent damage model and two definitions of stress intensity factor are proposed. The results of experiments and theoretical analysis show that the creep strain of tuff increases with increasing temperature under the same loading condition, and that the stress intensity factor is not only a function of stress states, but also of temperature.

Dwivedi et al. (2008) study the thermo-mechanical and transport properties of granites which is required to understand and model a number of processes in the earth crust such as folding, geothermal activity, magmatic intrusions, plate tectonics

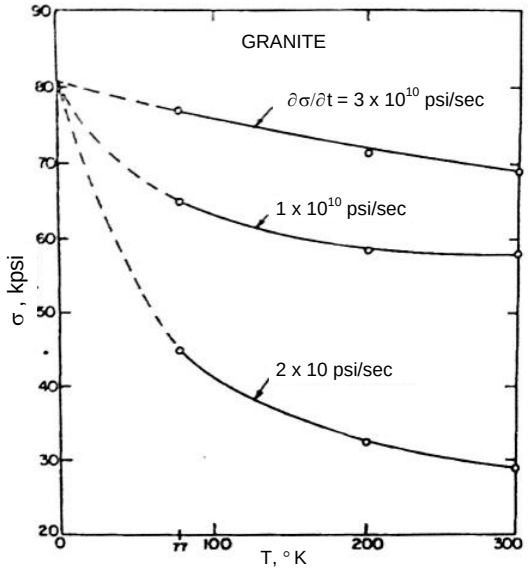

Figure 2.13 Effect of temperature and stress rate on the fracture strength on granite showing thermally activated fracture mechanism (Kumar, 1968).

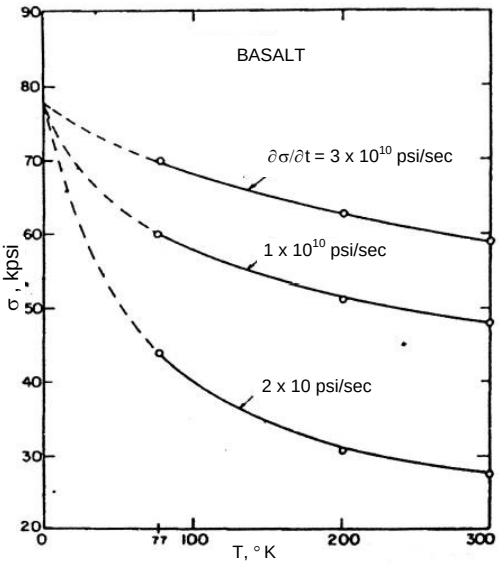

Figure 2.14 Effect of temperature and stress rate on the fracture strength on basalt showing thermally activated fracture mechanism (Kumar, 1968).

and nuclear waste disposal. Thermo-mechanical properties of Indian granite (IG) is studied various at high temperatures in the range of 30–160 °C, keeping in view the highest temperatures expected in underground nuclear waste repositories. These properties are Young's modulus, uniaxial compressive strength, tensile strength, Poisson's ratio, coefficient of linear thermal expansion, creep behaviour and the development of micro-crack on heating using scanning electron microscope (SEM). The results indicate that the temperature effect on creep under atmospheric pressure condition (0.1 MPa) was not observed up to 160 °C in the duration of 4 months for Indian pink granite. Permeability decreases with increase in temperature. Thermal conductivity and thermal diffusivity both decrease with increase in temperature. The decrease in thermal conductivity with temperature is high on increase of the confining pressure. On the other hand, specific heat increases with increase in temperature and

pressure up to 600 °C and the coefficient of linear thermal expansion increases with temperature up to 470 °C. Viscosity of molten granite decreases with increase in temperature. Ultimate compressive strength increases with increase in confining pressure. On the other hand, tensile strength of all granites decreases with increase in temperature for the reported temperature range 30–1050 °C. Normalized cohesion (c/c_0) and normalized angle of internal friction (ϕ/ϕ_0) both decrease with increase in temperature for all granites.

2.6 Loading rate effect on other rocks

Sangha and Dhir (1972) study the influence of strain rate on the strength, deformation and fracture properties of Lower Devonian sandstone are presented. Strain rates are varied between 2.5×10^{-3}/sec to 2.5×10^{-9}/sec. A new criterion, based on the incremental Poisson's ratio, capable of predicting both the long-term strength of a material and also able to establish whether a material under load is safe from long-term failure is suggested. This criterion is based on short-term creep tests and substantiated by the constant strain-rate strength results. Comparison of strength results obtained at different rates of loading and rates of straining show that for similar loading times to failure the constant rates of loading give slightly higher strength values. Modes of rupture are found to be independent of both loading methods but dependent upon time taken to reach strength failure.

Ray et al. (1999) describe the effect of cyclic loading and strain rate on the mechanical behaviour of sandstone. The results indicate that the percentage decrease in uniaxial compressive strength was found to increase with the increase in applied stress level and direct proportionality between the two parameters was found. The

uniaxial compressive strength of Chunar sandstone was determined at strain rates of 2.5×10^{1}/s, 2.5×10^{0} and 2.5×10^{-1}/s and found to be 99.5 MPa, 75.1 MPa and 64.0 MPa, respectively (Figure 2.15). A clear increase in uniaxial compressive strength was, therefore, observed with increase in strain rate. The failure strength was found to increase with the increase of strain rate and an abrupt increase in strength was noticed at the strain rate of 2.5×10^{1}/s. Fatigue stress was found to increase with the increase in strain rate, and Young's modulus was found to increase with the increase in strain rate (Figure 2.16).

Backers et al. (2003) studied the influence of loading rate on mechanical properties of rock and the resulting initiation and propagation of fractures. They investigated the influence of loading rate on fracture toughness, fracture roughness and microstructure of sandstone samples subjected to Mode I loading. Fracture toughness is dependent on the fracture velocity. At low velocities, fracture toughness, K_{IC}; remains almost constant. Exceeding a threshold of fracture velocity, fracture toughness increases significantly. Fracture roughness also increases with increasing loading rate.

Hashiba et al. (2006) study the loading-rate dependency for Tage tuff, Sanjome andesite and Akiyoshi marble. The loading-rate dependency of peak strength in these experiments shows a close relation with the creep stress-dependency of creep life. Under confining pressure, the corrected stress–strain curve, obtained by multiplying the stress of the complete stress–strain curve obtained at the fast strain rate by a constant determined by the ratio between the fast strain rate and slow strain rate, is nearly coincident with the stress–strain curve for the slow strain rate. This is an interesting result and represents new knowledge that may help elucidate failure

mechanisms in the post-failure region. The loading-rate dependency of stress in the alternating strain rate experiment was most clearly observed when the stress–strain curve becomes flat, parallel to the strain axis.

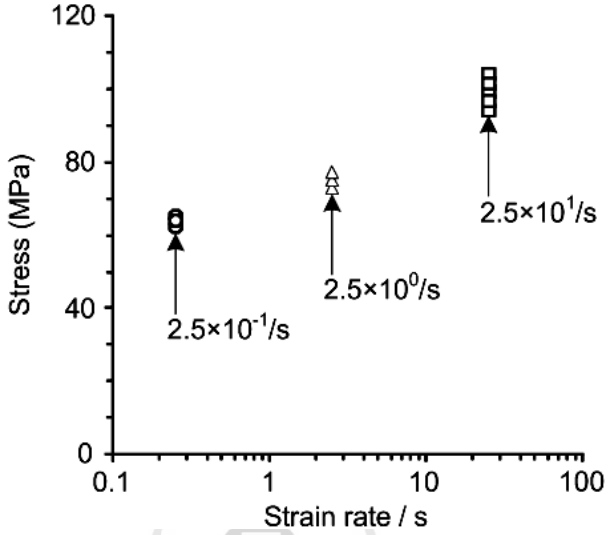

Figure 2.15 Stress as function of strain rate (Ray et al., 1999).

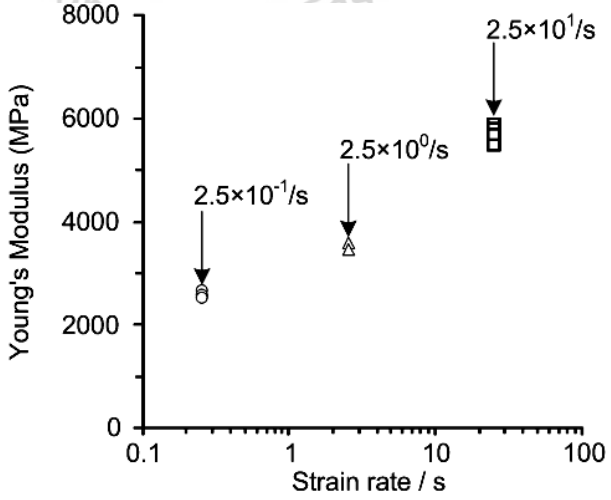

Figure 2.16 Young's modulus as function of strain rate (Ray et al., 1999).

Ma and Daemen (2006) study the strain rate dependent strength and stress-strain characteristics of a welded tuff. Results of 61 uniaxial compression tests on the welded Topopah Spring tuff are presented. The tests were carried out under constant strain rates at room temperature. Stress–strain analysis indicates that dilatancy and compaction start at about 50% of ultimate strength. A sudden stress drop occurs at about 90% of the ultimate strength, which indicates the onset of specimen failure. Both strength and peak axial strain decrease with strain rate as power functions. Based on the strain rate dependence of strength and peak axial strain, it is inferred that the elastic modulus is strain rate dependent. A relationship between stress, axial strain, and axial strain rate is developed. The parameters in this relation are estimated using multivariate regression to fit stress–axial strain–strain rate data.

Okubo et al. (2006) perform uniaxial compression tests and uniaxial tension tests on coal, with particular attention to two concerns. The first was to measure the loading rate dependence of the peak strength of coal. Anthracite samples were subjected to alternating slow and fast strain rates. Measured variations in stress during this process were used to estimate the loading rate dependence of peak strength. The second objective was to obtain complete stress–strain curves for coal under uniaxial tensile stress. It is difficult to hold samples secure during a tensile test; consequently, such curves have yet to be obtained. This study presents a successful application of the authors' method to the analysis of coal samples, yielding a complete stress–strain curve under tensile stress. The two methods presented here hold promise for application not only to anthracite but also to a wide variety of coals. It is possible to derive the values of the constants used in constitutive equations from

the obtained experimental results. The results obtained in the present study are the complete stress–strain curve for the uniaxial tension test showed ductility, with some residual strength. Comparison of the uniaxial tension strength with the conventional test of indirect tensile strength shows that the latter is 2–3 times higher than the uniaxial tension strength. The peak strength of coal has a relatively low dependence on strain rate under both uniaxial compressive stress and uniaxial tensile stress.

Fuenkajorn and Kenkhunthod (2010) study the influence of loading rate on deformability and compressive strength of three Thai sandstones. Uniaxial and triaxial compressive strength tests have been performed using a polyaxial load frame to assess the influence of loading rate on the strength and deformability of three Thai sandstones. The applied axial stresses are controlled at constant rates of 0.001, 0.01, 0.1, 1.0 and 10 MPa/s. The confining pressures are maintained constant at 0, 3, 7 and 12 MPa, are shown in Figure 2.17. The sandstone strengths and elastic moduli tend to increase exponentially with the loading rates. The effects seem to be independent of the confining pressures. An empirical loading rate dependent formulation of both deformability and shear strength is developed for the elastic and isotropic rocks. It is based on the assumption of constant distortional strain energy of the rock at failure under a given mean normal stress. The proposed multiaxial criterion well describes the sandstone strengths within the range of the loading rates used here. It seems reasonable that the derived loading rate dependent equations for deformability and shear strength are transferable to similar brittle isotropic intact rocks.

Huang and Liu (2013) study the effect of loading rate on the behavior of samples composed of coal and rock. To accurately evaluate the danger from rock bursts during coal mining, uniaxial compression tests of composed coal rock at

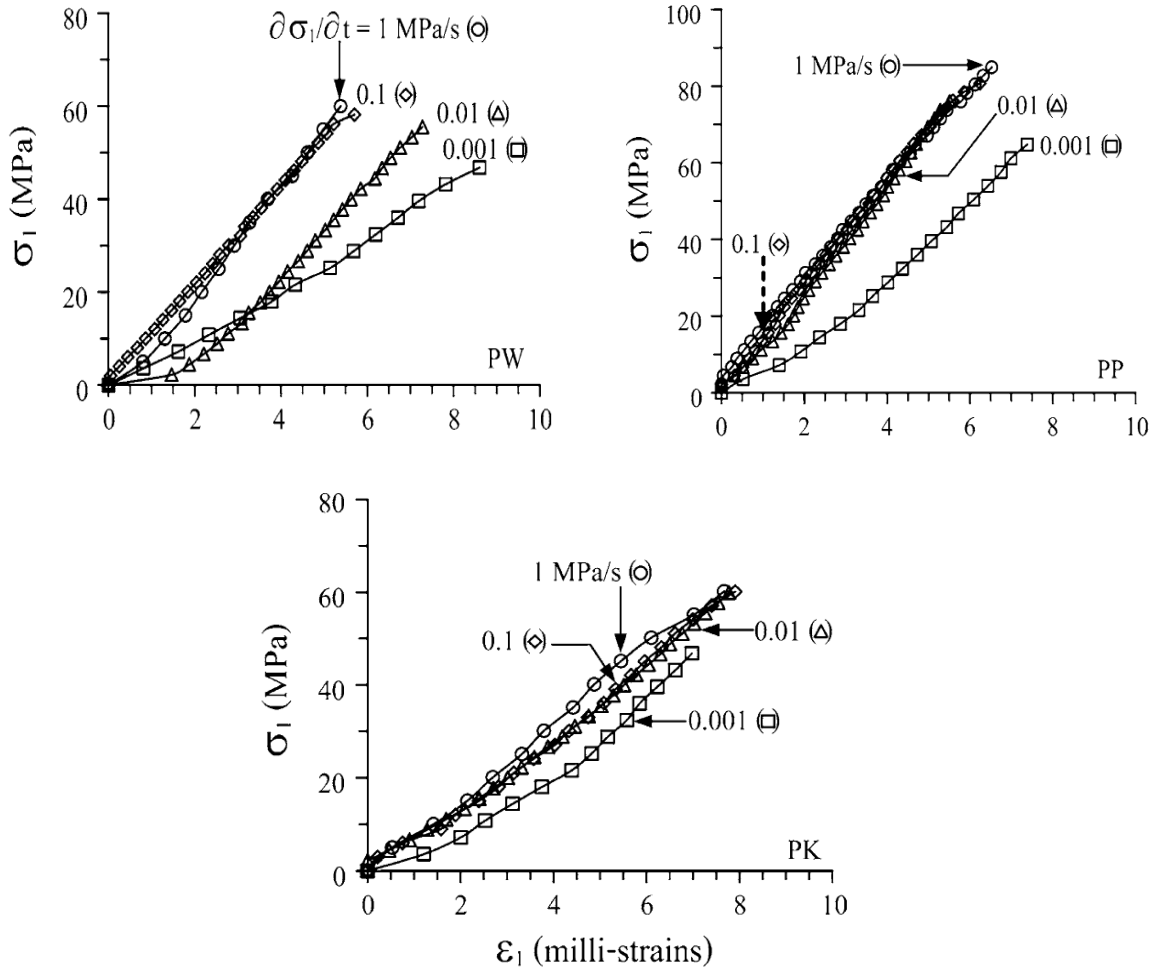

Figure 2.17 Uniaxial compressive strengths under loading rates varied from 0.001, 0.01, 0.1 and 1.0 MPa/s, for PW, PP and PK sandstones (Fuenkajorn and Kenkhunthod, 2010).

different loading rates were carried out. The effect of the rate and path of loading and unloading on the mechanical properties of the composed coal rock has been analyzed. The overall elastic modulus, peak strength, and residual strength of the composed coal rock lie among that of roof, coal, and floor. With an increase of loading rate, the strain increment of the composed coal rock in the elastic phase, the plastic phase, and the failure phase gradually increased, and the strain at the peak point rose linearly

shown in Figure 2.18. The strain at the point of peak strength of the composed coal rock increases linearly with the increase of loading rate shown in Figure 2.19.

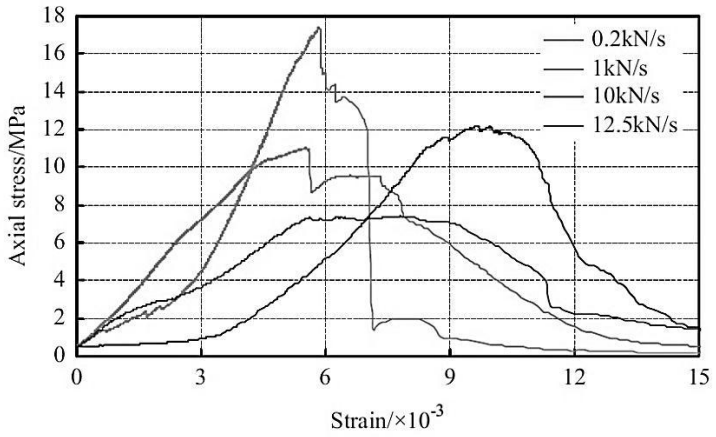

Figure 2.18 Overall stress–strain curves of the composed coal rock at different loading rates (Huang and Liu, 2013).

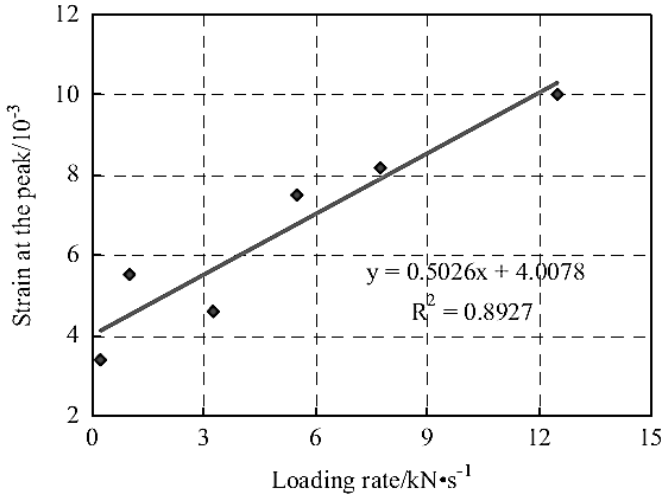

Figure 2.19 The relationship between loading rate and strain at the point of peak strength (Huang and Liu, 2013).

The relationships between loading rate and elastic modulus in the phases of first loading, unloading, and reloading are shown in Figure 2.20. Owing to the discreteness of experimental results, the elastic moduli in the phases of first loading, unloading, and reloading at the loading rate of 3.25 kN/s are greater than those at other loading rates on the whole. At the same loading rate, the relationship among the elastic moduli in the phases of first loading, first unloading, and reloading is $E_1<E_3<E_2$, which is determined by the physical and mechanical properties of the coal and rock.

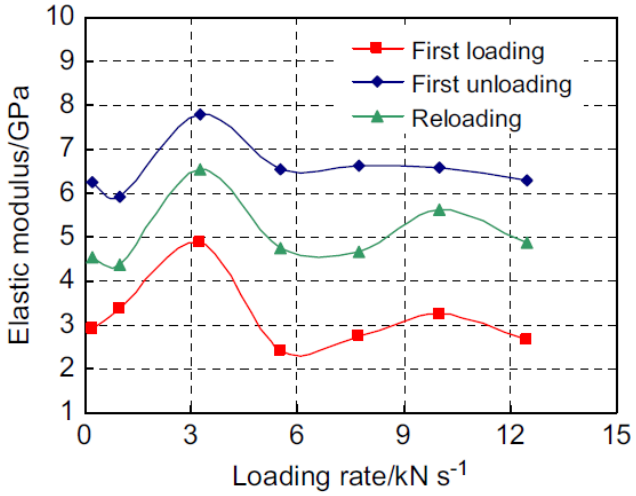

Figure 2.20 The relationship between loading rate and elastic modulus in the phases of first loading, first unloading, and reloading (Huang and Liu, 2013).

CHAPTER III

SAMPLE PREPARATION

3.1 Sample preparation

The salt specimens are prepared from 47 mm diameter cores drilled from the depths ranging between 270 m and 330 m by Siam Submanee Co., Ltd. in the northeast of Thailand (Figure 3.1). The salt belongs to the Lower Salt member of the Maha Sarakham formation. The cores are drilled and dried-cut to cylindrical shaped specimens with nominal dimension (Figures 3.2). A total of 30 samples have been prepared. Tabakh et al. (1999) and Warren (1999) give detailed descriptions of the salt and geology of the basin. Sample preparation is conducted in laboratory facility at the Suranaree University of Technology. Table 3.1 summarizes the specimen number, depth, dimensions and density. The average density of salt specimens is 2.20±0.02 g/cm^3. After preparation the specimens are wrapped with plastic sheet at all time to prevent it from subjecting to the surrounding humidity. No bedding is observed in the specimens.

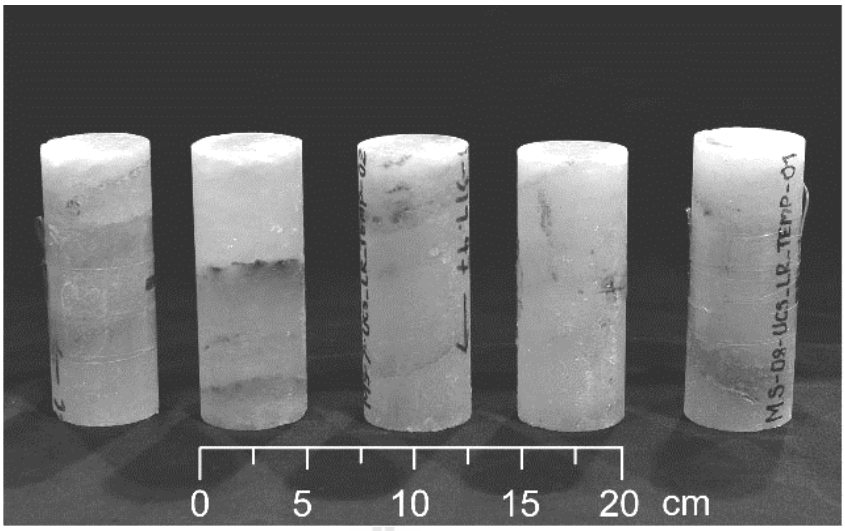

Figure 3.1 Some salt cores from the depth ranging between 270 m and 330 m by Siam Submanee Co,. Ltd.

Figure 3.2 Salt core is dry-cut by a cutting device.

Table 3.1 Specimen dimensions prepared for uniaxial compression testing.

Specimen No.	Depth (m)	Diameter (mm)	Height (mm)	Density (g/cm^3)
MS-17-UCS_LR_TEMP-01	272.01 - 272.13	47.16	118.00	2.17
MS-17-UCS_LR_TEMP-02	272.13 - 272.25	47.06	118.20	2.17
MS-12-UCS_LR_TEMP-02	281.40 - 281.52	47.36	117.20	2.14
MS-01-UCS_LR_TEMP-01	371.02 - 317.14	47.50	118.44	2.16
MS-02-UCS_LR_TEMP-01	314.65 - 314.76	47.46	117.40	2.14
MS-05-UCS_LR_TEMP-02	318.64 - 318.64	47.52	117.41	2.15
MS-07-UCS_LR_TEMP-01	319.01 - 319.13	47.40	118.22	2.16
MS-07-UCS_LR_TEMP-03	319.25 - 319.37	47.36	118.28	2.15
MS-10-UCS_LR_TEMP-01	313.38 - 313.50	47.46	118.46	2.15
MS-10-UCS_LR_TEMP-03	313.15 - 313.27	47.54	119.90	2.13
MS-11-UCS_LR_TEMP-02	325.54 - 325.66	47.46	117.32	2.15
MS-14-UCS_LR_TEMP-01	275.72 - 275.96	47.18	118.42	2.18
MS-14-UCS_LR_TEMP-02	275.84 - 275.96	47.06	117.14	2.17
MS-15-UCS_LR_TEMP-01	276.27 - 276.39	47.22	118.80	2.15
MS-23-UCS_LR_TEMP-01	312.10 - 312.58	47.20	119.04	2.12
MS-23-UCS_LR_TEMP-04	295.20 - 296.01	47.56	118.50	2.14
Average				2.20 ± 0.02

CHAPTER IV

LABORATORY TESTING

4.1 Introduction

The objective of this section is to experimentally determine the effects of loading rate on compressive strength and deformability of the Maha Sarakham salt under temperatures ranging from 273 to 373 Kelvin. This chapter describes the test method and results.

4.2 Test method

Uniaxial compression test is carried out. The applied loading rates are constant at of 0.0001, 0.001, 0.01 and 0.1 MPa/s. The digital strain meter indicator (TC-31K) connected with an electronic load cell is used to record the load increment. The load at failure is recorded to determine the salt compressive strength. The specimen deformations are monitored with four dial gages to determine the increase of compressive strains. Photographs are taken of the failed specimens.

4.2.1 Low temperature testing

The salt specimen is placed in the consolidation load frame and installed inside the cooling system for low temperature test at 273 Kelvin. The salt specimen is cooled for 48 hours before starts loading. The cooling system is fabricated to test the salt specimen while loading. It can cool the salt specimens down to 273 K. Figure 4.1 shows the specimen placed in the cooling system for

low temperature test at 273 Kelvin. The specimen installation, equipment setup and loading are completed within 4 minutes. The changes of specimen temperatures between before and after testing are less than 5 Kelvin. As a result the specimen temperatures are assumed to be uniform and constant with time during the mechanical testing (i.e., isothermal condition).

4.2.2 Ambient temperature testing

For the uniaxial compression testing under ambient temperature (303 Kelvin), the salt specimen is placed in a consolidation load frame and loaded diametrically until failure as shown in Figure 4.2. The electronic load cell is used to record the load increase.

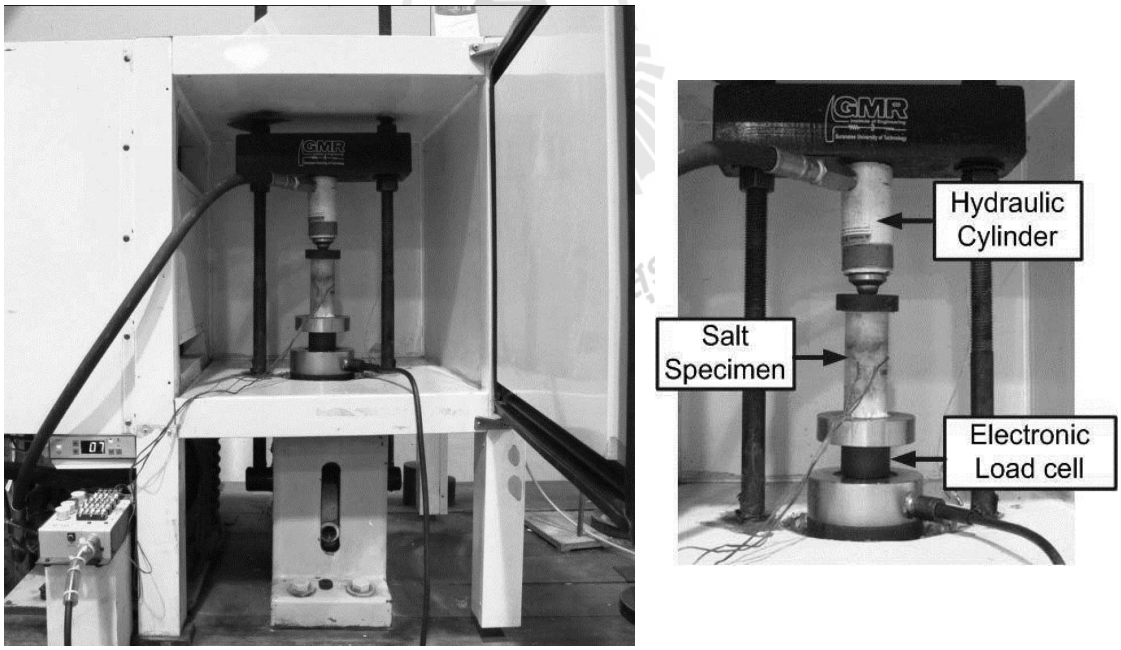

Figure 4.1 A salt specimen placed in the consolidation load frame and inside the cooling system for low temperature test at 273 K.

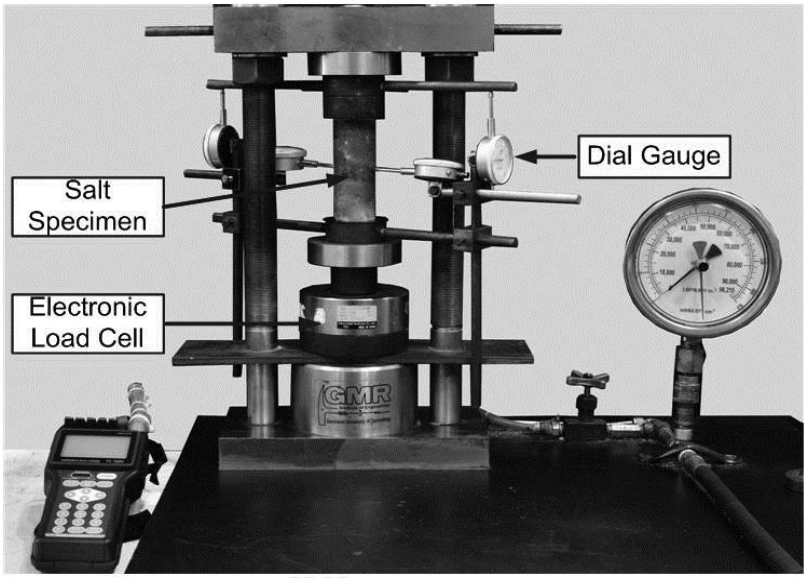

Figure 4.2 Salt specimen placed in a consolidation load frame under room temperature (303 K).

4.2.3 High temperature testing

For the high temperature testing a heating tape with temperature regulator is used to apply constant elevated temperatures to the specimens from 343 to 373 Kelvin. The salt specimens are wrapped with heating tape, foil and insulation while loading as shown in Figure 4.3. A heating tape can heat the salt specimens up to 373 Kelvin. The specimen is installed with the heating system for 24 hours before loading started.

4.3 Test results

Figure 4.4 shows the stress-strain curves monitored from some of the salt specimens under different stress rates and temperatures. Table 4.1 gives the test results. The specimens tend to show nonlinear behavior, particularly under high

temperatures. All post-test specimens show shear failure mode (Figure 4.5). Under the same loading rate ($\partial\sigma_1/\partial t$), the compressive strength (σ_c) decreases with increasing specimen temperatures. The mean stresses (σ_m) and strains (ε_m) and octahedral shear stresses ($\tau_{oct,f}$) and shear strains ($\gamma_{oct,f}$) at failure are determined using the following relations (Jaeger et al., 2007):

$$\sigma_m = (\sigma_1 + \sigma_2 + \sigma_3)/3 \tag{4.1}$$

$$\varepsilon_m = (\varepsilon_1 + \varepsilon_2 + \varepsilon_3)/3 \tag{4.2}$$

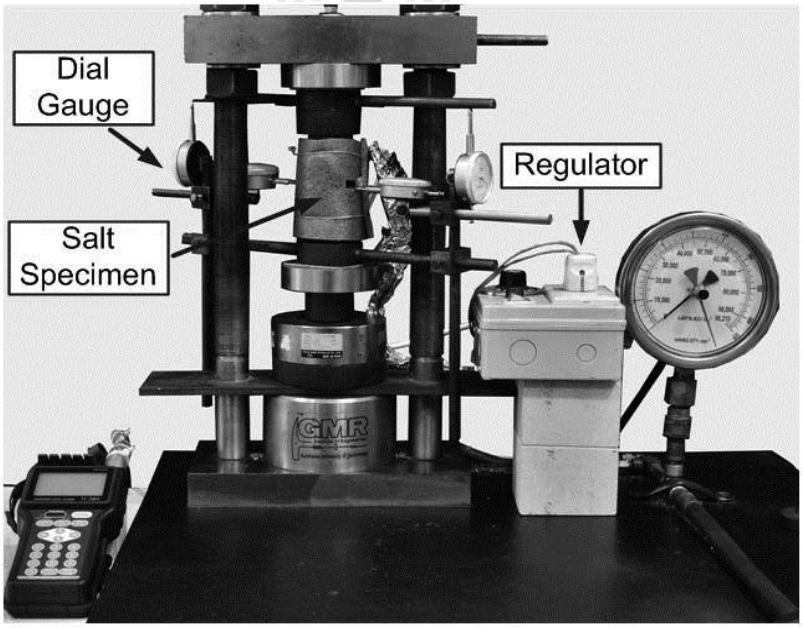

Figure 4.3 Salt specimens wrapped with the heating tape and insulator for high temperature testing at 343 and 373 K.

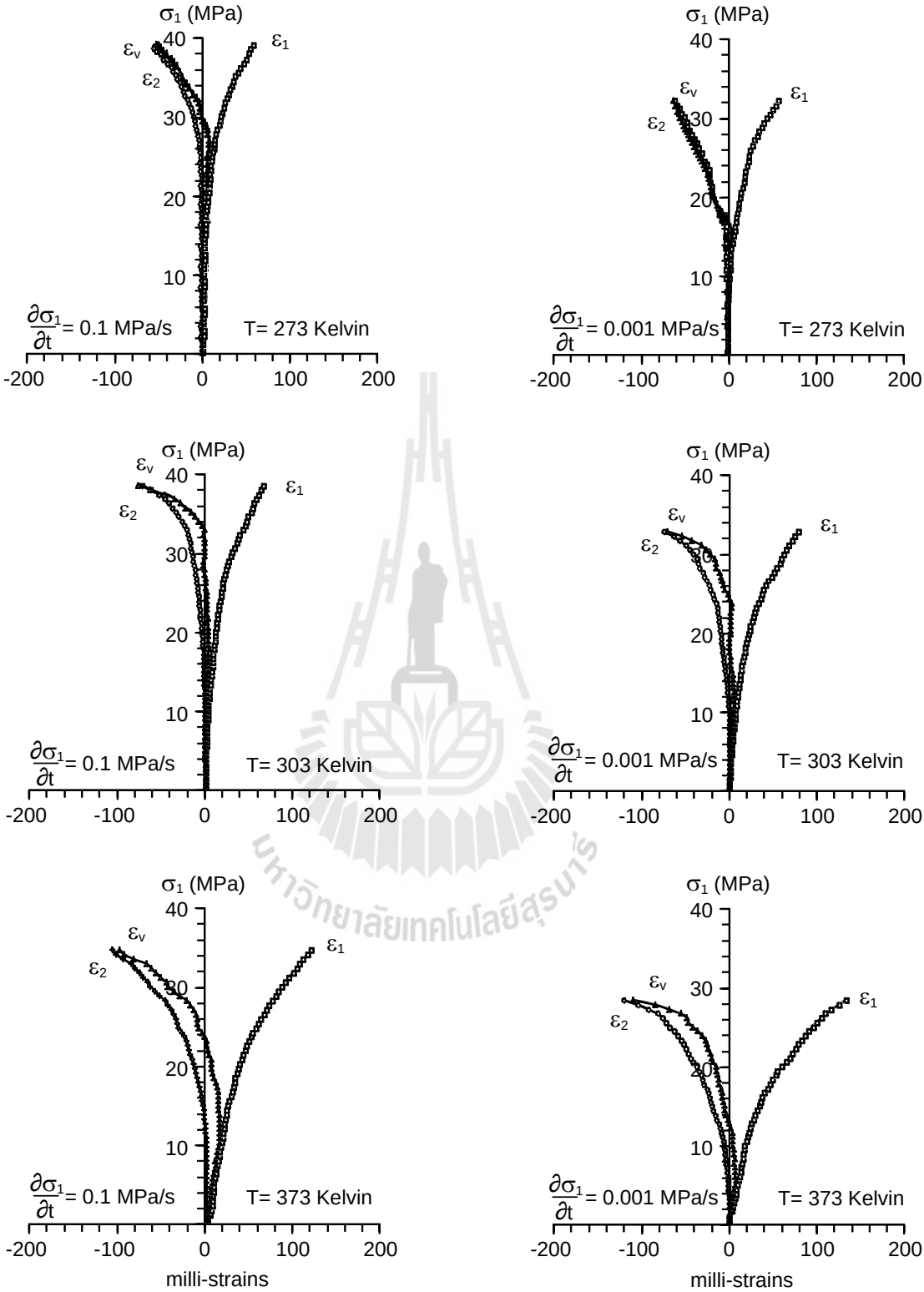

Figure 4.4 Stress-strain curves obtained from some salt specimens with different loading rates ($\partial\sigma_1/\partial t$) and temperatures (T).

Table 4.1 Salt strengths under various loading rates and temperatures.

Average Temperature (Kelvin)	Loading rate (MPa/s)	Uniaxial compressive strength (MPa)	Mean stress (MPa)
273	0.1	38.79	12.93
	0.01	34.94	11.65
	0.001	33.22	11.07
	0.0001	29.78	9.93
303	0.1	37.23	12.41
	0.01	34.56	11.52
	0.001	32.59	10.86
	0.0001	29.19	9.73
343	0.1	35.78	11.93
	0.01	33.51	11.17
	0.001	29.69	9.90
	0.0001	26.58	8.86
373	0.1	34.60	11.53
	0.01	31.51	10.50
	0.001	28.11	9.37
	0.0001	25.16	8.39

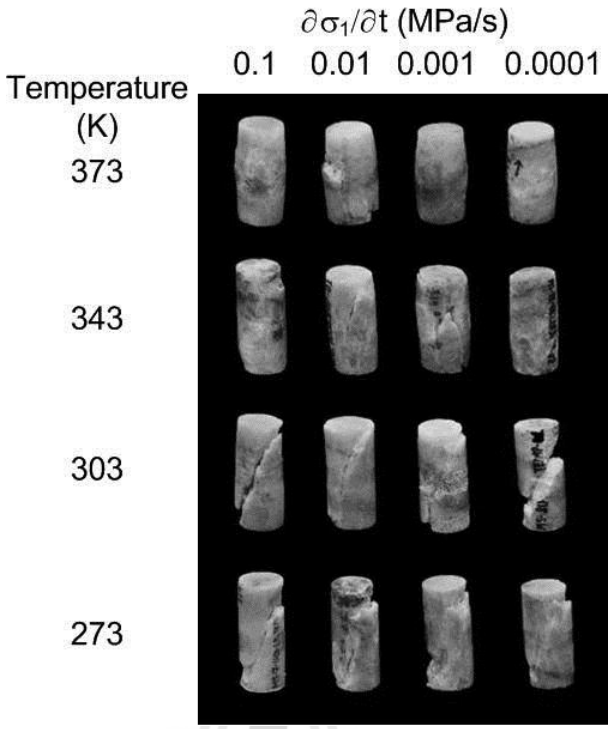

Figure 4.5 Post-test specimens from uniaxial compressive strength testing under different loading rates ($\partial\sigma_1/\partial t$) and temperatures (T).

$$\tau_{oct} = (1/3)\left[(\sigma_1 - \sigma_2)^2 + (\sigma_1 - \sigma_3)^2 + (\sigma_2 - \sigma_3)^2\right]^{1/2} \quad (4.3)$$

$$\gamma_{oct} = (1/3)\left[(\varepsilon_1 - \varepsilon_2)^2 + (\varepsilon_1 - \varepsilon_3)^2 + (\varepsilon_2 - \varepsilon_3)^2\right]^{1/2} \quad (4.4)$$

where σ_1, σ_2 and σ_3 are the major, intermediate and minor principal stresses at failure.

The applied octahedral shear stresses are plotted as a function of octahedral shear strain in Figure 4.6. The shear stress-strain relations are nonlinear, particularly under

low loading rates and high temperatures. Higher shear strengths and lower shear strains are observed under low stress rates and high temperatures.

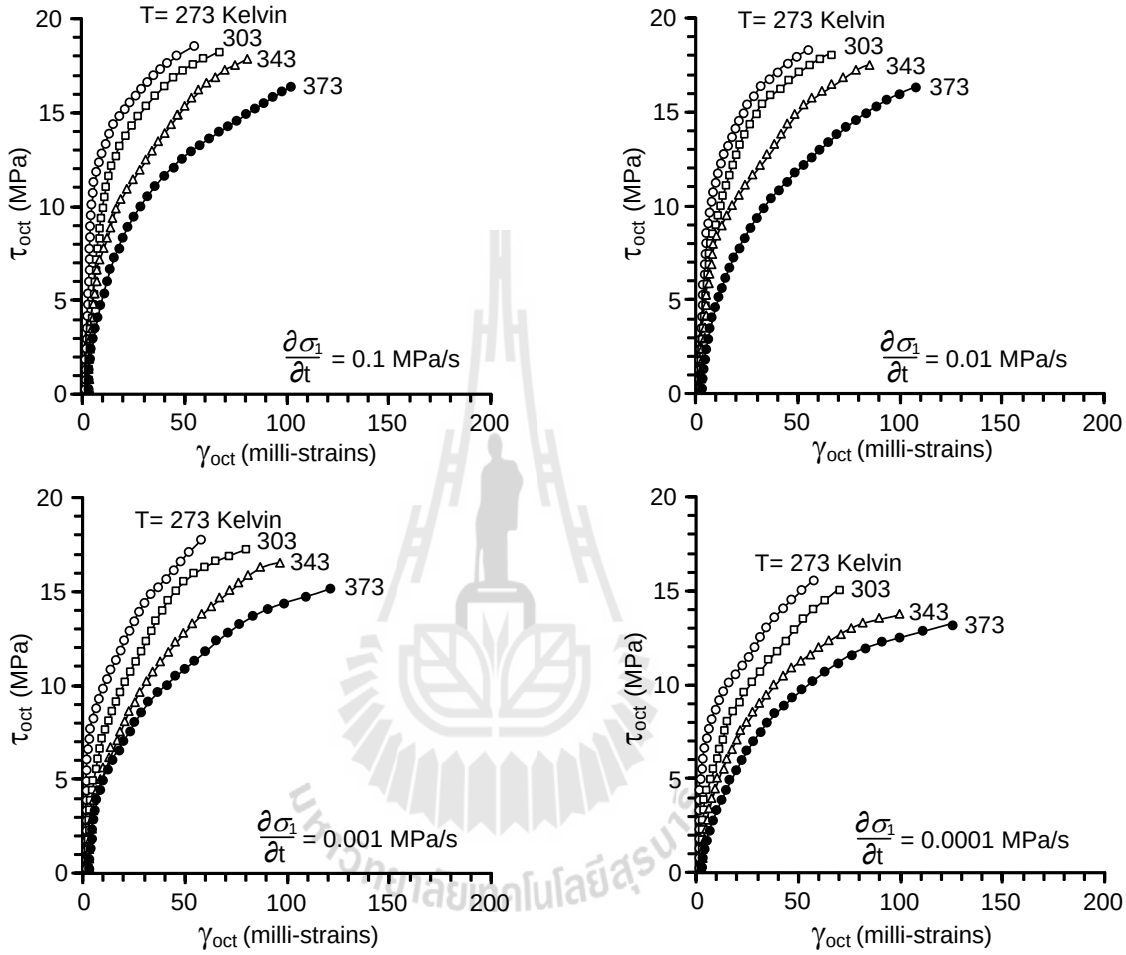

Figure 4.6 Octahedral shear stress (τ_{oct}) as a function of octahedral shear strain (γ_{oct}) for various loading rates ($\partial\sigma_1/\partial t$) and temperatures (T).

CHAPTER V

CALIBRATION OF ELASTIC AND CREEP PARAMETERS

5.1 Objectives

The purpose of this chapter is to describe the calibration results of the elastic and transient creep parameters. The regression analysis of the proposed compressive creep strain equation with the IBM SPSS Statistics 19 (Wendai, 2000) is performed to determine the elastic and creep parameters. Results from laboratory are used to predict the octahedral shear stresses under various octahedral shear stress rates and temperatures. To incorporate the thermal and rate (time-dependent) effects into a strength criterion the distortional strain energy of the salt is calculated as a function of the mean strain energy density.

5.2 Elastic properties of the Maha Sarakham salt

The elastic modulus and Poisson's ratio for each specimen are determined from the tangent of the stress-strain curves at 40% failure stress. Based on this calculation the elastic modulus of the salt appears to increase with loading rate and decrease with temperature (Figure 5.1). It ranges from 11 to 29 GPa. The poisson's ratio of the salt range from 0.31 to 0.42, and tend to be independent of the loading rate and temperature (Figure 5.2).

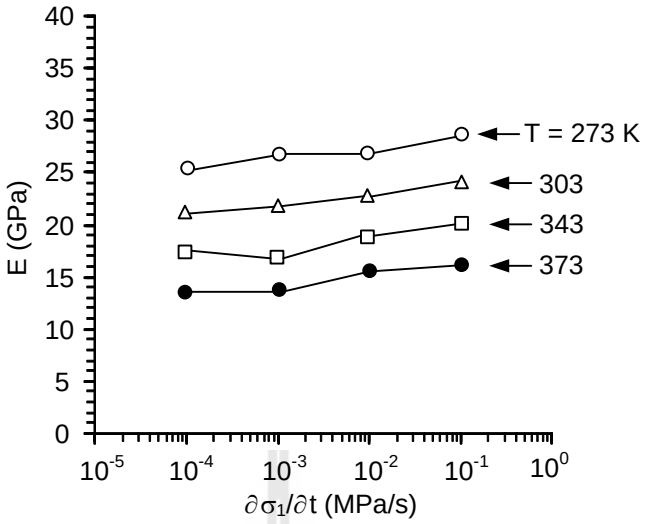

Figure 5.1 Elastic modulus (E) as a function of loading rate ($\partial\sigma_1/\partial t$) for various temperatures (T).

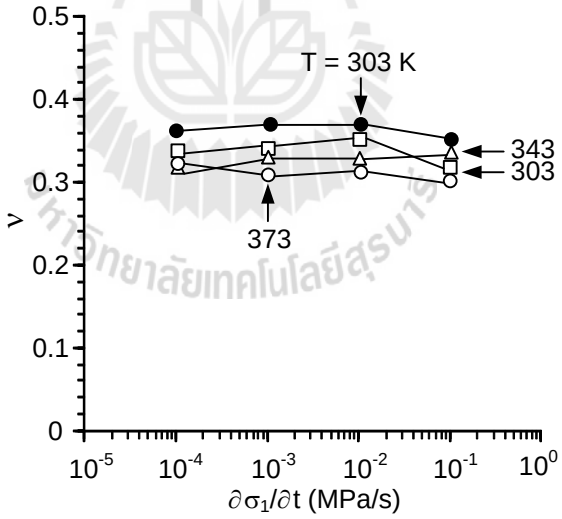

Figure 5.2 Poisson's ratio (ν) as a function of loading rate ($\partial\sigma_1/\partial t$) for various temperatures (T).

The elastic modulus and poisson's ratio of the same salt determined by Fuenkajorn et al. (2012) under various loading rate are increase with loading rate and poisson's ratio tend to be independent of the loading rate, Sriapai et al. (2012) under various temperature are decrease with temperature and Poisson's ratio tend to be independent of the temperatures. Their results agree reasonably well with the results obtained here.

The elastic moduli for the all tested rock salt are plotted as a function of loading rates and temperatures. The empirical equations can be written as:

$$E = \ln(\partial\sigma_c/\partial t)\cdot\chi + \exp(\xi/T) + \ell \qquad \text{(GPa)} \qquad (5.1)$$

where E is the elastic modulus (GPa), χ, ξ and ℓ are empirical constants. The unit of loading rate ($\partial\sigma_c/\partial t$) and temperature (T) are MPa/s and Kelvin. For the Maha Sarakham salt the empirical constants in equation (5.1) are defined by the regression analysis as: χ = 0.542 s^{-1}; ξ = 840.480 MPa·Kelvin; ℓ = 9.285 MPa. Good correlation is obtained (R^2 = 0.976). Figure 5.3 compares the test results with the back predictions from the proposed equation.

5.3 Total compressive strain

The total compressive strain (ε_c) is divided here into two parts; elastic strain (ε_c^e, linear and recoverable strain) and plastic creep strain (ε_c^c, time-dependent and non-recoverable strain):

$$\varepsilon_c = \varepsilon_c^e + \varepsilon_c^c \qquad (5.2)$$

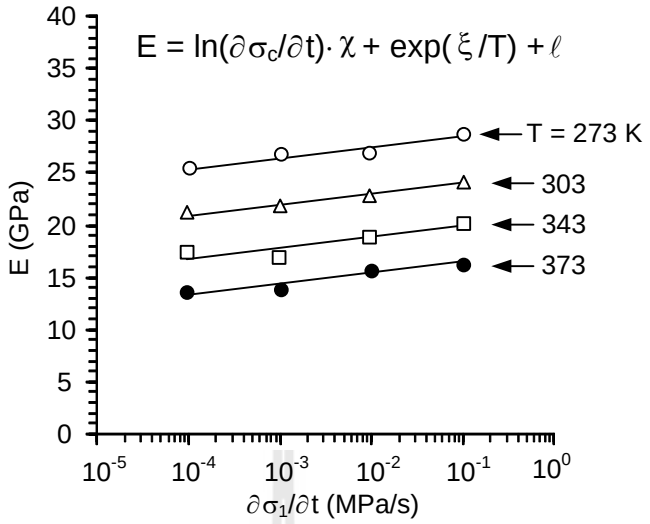

Figure 5.3 Elastic modulus as a function of loading rates and temperatures. Comparisons between test results (points) and back predictions (lines).

The elastic strain can be calculated from the current stress state using classical elastic theory by Jaeger et al. (2007):

$$\varepsilon_c^e = \frac{\sigma_c}{E} \tag{5.3}$$

where σ_c is the compressive stress, E is the compressive elastic modulus. The exponential creep law is used to describe time-dependent strain of the salt. Under isothermal condition the exponential law can describe the creep strain (ε_c^c) as a function of constant stress, constant temperature and time (Yang et al., 1999) as follows:

$$\varepsilon_c^c = \alpha \cdot \sigma_c^{\beta} \cdot t^{\kappa} \cdot \exp\left(-\lambda/T\right) \tag{5.4}$$

where α, β, κ and λ are empirical constants, t is elapsed time and T is the constant temperature in Kelvin. Substituting Equations (5.3) through (5.4) into (5.2) we obtain:

$$\varepsilon_c = \frac{\sigma_c}{E} + \alpha \cdot \sigma_c^{\beta} \cdot t^{\kappa} \cdot \exp\left(-\lambda/T\right) \tag{5.5}$$

Similarly the creep parameters can also be derived in the forms of the octahedral shear strain:

$$\gamma_{oct} = \frac{\tau_{oct}}{2G} + \alpha \cdot \tau_{oct}^{\beta} \cdot t^{\kappa} \cdot \exp\left(-\lambda/T\right) \tag{5.6}$$

where γ_{oct} is the octahedral shear strain (millistrain), τ_{oct} is the octahedral shear stress (MPa), G is shear modulus (GPa), α is stress constant, β is stress exponent, T is temperature (Kelvin), t is time (second), κ is time exponent and λ is temperature constant.

For the stress-rate controlled condition the octahedral shear stress at any loading time (t) can be expressed as:

$$\gamma_{oct} = \frac{\dot{\tau}_{oct}}{2G} + \alpha \cdot \exp\left(-\lambda/T\right) \cdot \dot{\tau}_{oct}^{\beta} \cdot t^{\beta+\kappa} \tag{5.7}$$

where G is shear modulus (GPa). Assuming that the salt elasticity varies linear with temperature (Archeeploha and Fuenkajorn, 2012); the following equation is proposed:

$$G = -\psi \cdot T + G_0 \tag{5.8}$$

where G_0 is shear modulus at zero Kelvin and ψ is the empirical constant. Substitute equation (5.8) into (5.7) we obtain:

$$\gamma_{oct} = \frac{\dot{\tau}_{oct}}{2\left(-\psi \cdot T + G_0\right)} + \alpha \cdot \dot{\tau}_{oct}^{\beta} \cdot t^{(\beta+\kappa)} \cdot \exp\left(-\lambda/T\right) \tag{5.9}$$

Regression analysis of equation (5.9) by using the test data is performed to determine the elastic and creep parameters (Table 5.1). For the Maha Sarakham salt they are defined as ψ = -54.044 GPa·Kelvin^{-1}; G_0 = 25.822 GPa; α = 0.01 GPa^{-1}; β = 2.018; κ = 0.129; λ = 1559.242 Kelvin. Good correlation (R^2 = 0.954) between the proposed equation and the test data is obtained. Figure 5.4 compares the test data with the back predictions. This equation can be used to predict the time-dependent deformation of salt under various constants temperatures.

5.4 Strength criterion

5.4.1 Salt Compressive Strength

An empirical equation is proposed to predict the salt compressive strengths under various loading rates and temperatures:

$$\sigma_c = \ln(\partial\sigma_c/\partial t) \cdot \delta + \exp(\omega/T) + \varsigma \qquad \text{(MPa)} \tag{5.10}$$

where σ_c is the salt compressive strength (MPa), δ, ω and ς are empirical constants. The unit of loading rate ($\partial\sigma_c/\partial t$) and temperature (T) are MPa/s and Kelvin. For the

Maha Sarakham salt the empirical constants in equation (5.10) are defined by the regression analysis as: δ = 1.300 s^{-1}; ω = 605.764 MPa·Kelvin; ς = 32.968 MPa. Good correlation is obtained (R^2 = 0.960). Figure 5.5 compares the test results with the back predictions from the proposed equation.

The variation of the shear strengths can be observed from the τ_{oct} - σ_m diagram, as shown in Figure 5.6. The linear relation between the octahedral shears strength and the mean stress at failure and can be best represented by:

$$\tau_{oct,f} = 1.412 \cdot \sigma_m + 0.022 \quad \text{(MPa)} \quad (5.11)$$

5.4.2 Octahedral shear strength and shear rate relation

The octahedral shear stress at failure is calculated from the principal stresses at failure, as shown in equation (4.3). The octahedral shear stress and shear strains at dilation can be calculated from the major principal stresses and the three principal strains at dilation as follows.

Table 5.1 Parameters calibrated from uniaxial compression test results.

Parameters	Unit	Values	R^2
G_0	GPa	25.822	0.954
ψ	GPa·Kelvin^{-1}	-54.044	
α	GPa^{-1}	0.010	
β	-	2.018	
κ	-	0.129	
λ	Kelvin	1559.242	

$$\tau_{oct,d} = (1/3)\left[(\sigma_{1,d} - \sigma_{2,d})^2 + (\sigma_{1,d} - \sigma_{3,d})^2 + (\sigma_{2,d} - \sigma_{3,d})^2\right]^{1/2} \quad (5.12)$$

$$\gamma_{oct,d} = (1/3)\left[(\varepsilon_{1,d} - \varepsilon_{2,d})^2 + (\varepsilon_{1,d} - \varepsilon_{3,d})^2 + (\varepsilon_{2,d} - \varepsilon_{3,d})^2\right]^{1/2} \quad (5.13)$$

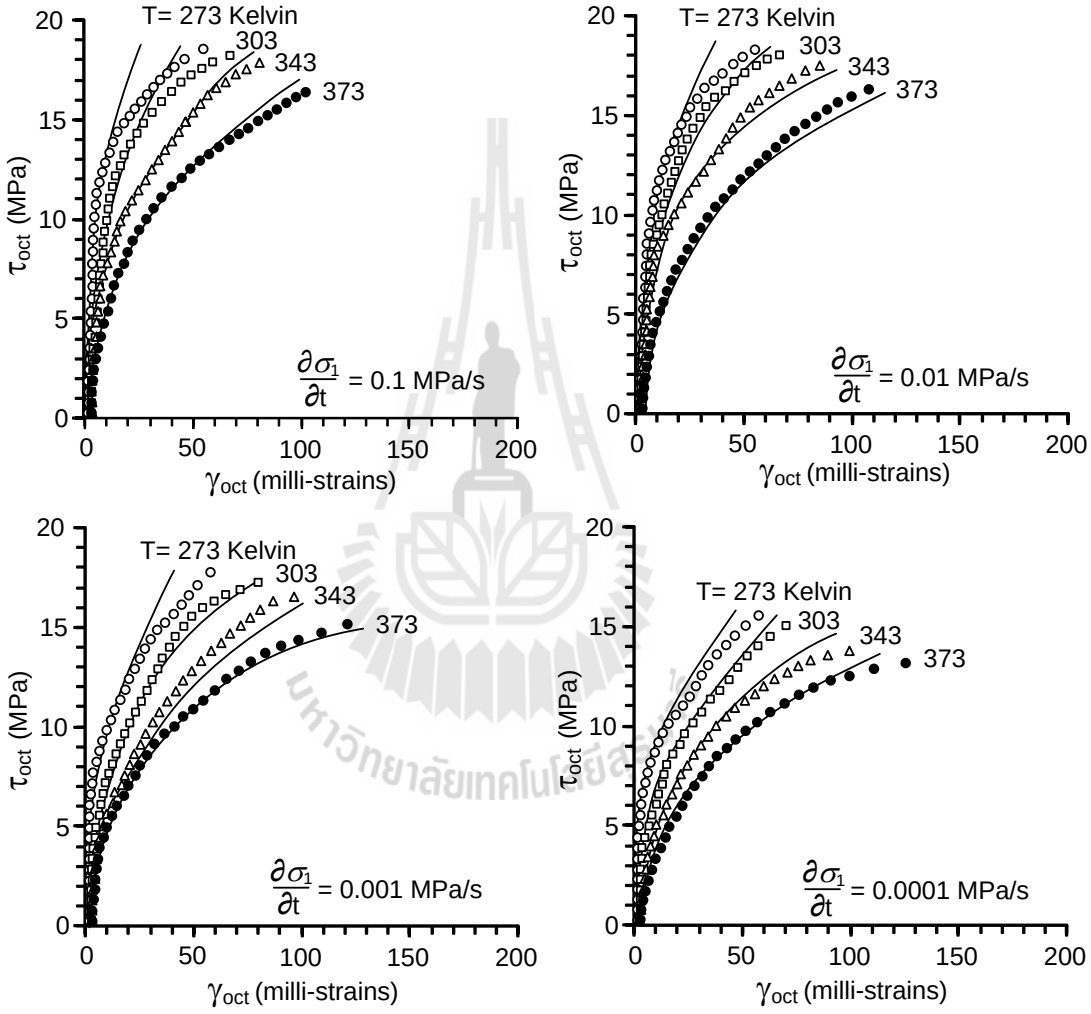

Figure 5.4 Octahedral shear stress–strain relations, test results (points) and back predictions (lines).

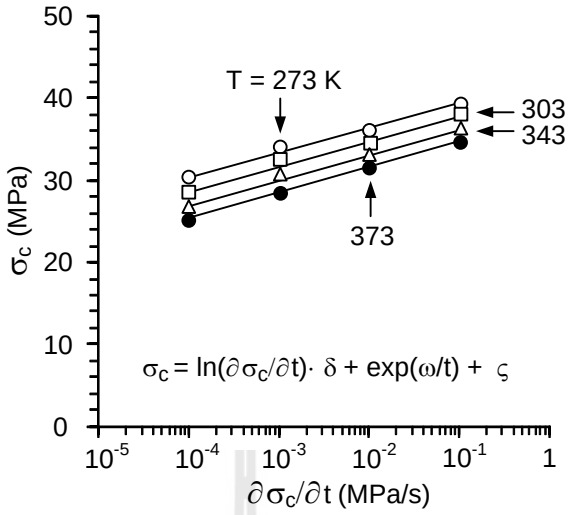

Figure 5.5 Uniaxial compressive strengths as a function of loading rates for various temperatures. Comparisons between test results (points) and back predictions (lines).

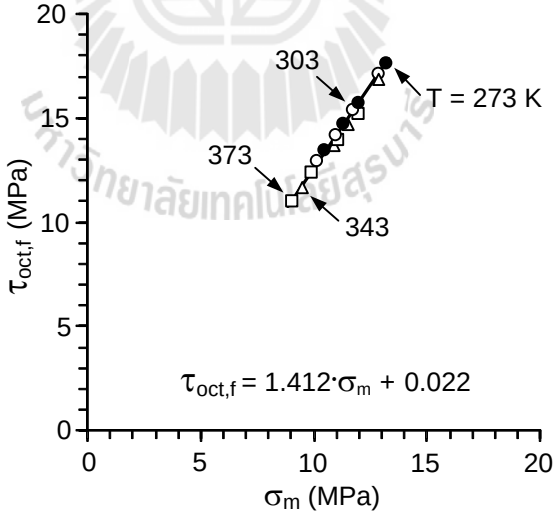

Figure 5.6 Octahedral shear stress at failure ($\tau_{oct,f}$) of salt as a function of mean stress (σ_m).

where $\sigma_{1,d}$ is the magnitude of the major principal stress at dilation starting to occur, and $\varepsilon_{1,d}$, $\varepsilon_{2,d}$ and $\varepsilon_{3,d}$ are the principal strains at dilation. Here the octahedral shear stresses at failure ($\tau_{oct,f}$) and at dilation ($\tau_{oct,d}$) are plotted as a function of the shear rate ($\partial\tau_{oct}/\partial t$) in Figures 5.7 and 5.8. The shear rate is determined by taking a derivative of equation (4.3) with respect to time (t). Since σ_2 and σ_3 are constant with time here, the following relation is obtained:

$$\partial\tau_{oct}/\partial t = (\sqrt{2}/3)\partial\sigma_1/\partial t \qquad (5.14)$$

An empirical equation is proposed to predict the octahedral shear stresses under various octahedral shear stress rates and temperatures:

$$\tau_{oct,f} = \ln(\partial\tau_{oct}/\partial t)\cdot ə + \exp(\eta/T) + ı \quad \text{(MPa)} \qquad (5.15)$$

$$\tau_{oct,d} = \ln(\partial\tau_{oct}/\partial t)\cdot ə' + \exp(\eta'/T) + ı' \quad \text{(MPa)} \qquad (5.16)$$

where ə, ə′, η, η′, ı and ı′ are empirical constants for the salt at failure and dilation, respectively. The unit of shear rate ($\partial\tau_{oct}/\partial t$) and temperature (T) are MPa/s and Kelvin. For the Maha Sarakham salt the empirical constants in equation (5.15) and (5.16) are defined by regression analysis as: ə = 0.613 s^{-1}; ə′ = 0.393s^{-1}; η = 460.323 MPa·Kelvin ; η′ = 421.015 MPa·Kelvin; ı = 14.936 MPa and ı′ = 5.766 MPa. Good correlation is obtained (R^2 = 0.962 at failure and R^2 = 0.874 at dilation). Figures 5.7 and 5.8 compare the test results with back predictions from the proposed equation.

5.4.3 Octahedral shear strength and shear strain relation

The octahedral shear strength and dilation criteria that can take the corresponding shear strain into account. From the test results the octahedral shear

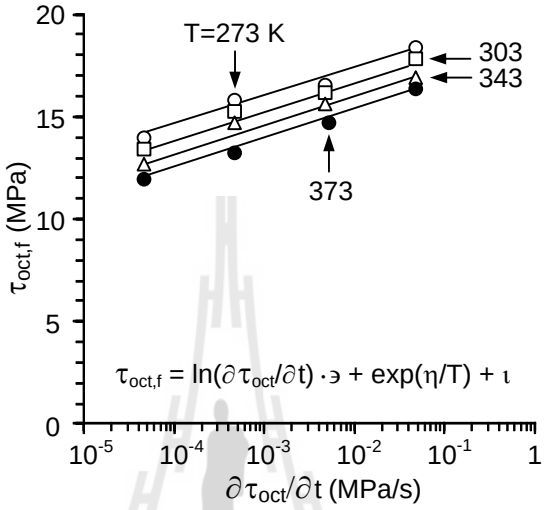

Figure 5.7 Octahedral shear stress at failure as a function of octahedral shear stress rate for various temperatures.

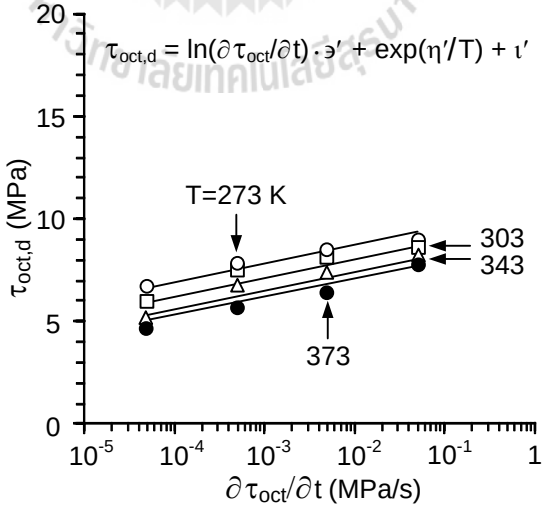

Figure 5.8 Octahedral shear stress at dilation as a function of octahedral shear stress rate for various temperatures.

stress can be calculated as a function of shear strain for various shear rates and temperatures as shown in Figures 5.9 and 5.10. The empirical equations can be written as:

$$\tau_{oct,f} = \varpi \cdot \gamma_{oct,f}^{\ \vartheta} + \ln(\partial\tau_{oct}/\partial t) \cdot \zeta + \exp(\varphi/T) \qquad \text{(MPa)} \qquad (5.17)$$

$$\tau_{oct,d} = \varpi' \cdot \gamma_{oct,d}^{\ \vartheta'} + \ln(\partial\tau_{oct}/\partial t) \cdot \zeta' + \exp(\varphi'/T) \qquad \text{(MPa)} \qquad (5.18)$$

where ϖ, ϖ', ϑ, ϑ', ζ, ζ', φ are φ' are empirical constants for the salt at failure and dilation, respectively. The unit of shear strain (γ_{oct}), shear rate ($\partial\tau_{oct}/\partial t$) and temperature (T) are strain, MPa/s and Kelvin. For the Maha Sarakham salt the empirical constants in equation (5.17) and (5.18) are defined by regression analysis as: ϖ = 37.500 MPa; ϖ' = 17.169 MPa; ϑ = -0.165; ϑ' = -0.165; ζ = 0.548 s^{-1}; ζ' = 0.265 s^{-1}; φ = -175.119 MPa·Kelvin and φ'=-238.562 MPa·Kelvin. Good correlation is obtained (R^2 = 0.979 at failure and R^2 = 0.970 at dilation). Figures 5.9 and 5.10 compare the test results with back predictions from the proposed equation.

5.5 Strain energy density criterion

The strain energy density principle is applied to describe the salt strength and deformability under different loading rates and temperatures. A similar approach has been used by Fuenkajorn et al. (2012) to derive a loading rate-dependent strength for salt. The distortional strain energy at failure (W_d) and at dilation ($W_{d,d}$) can be calculated from the octahedral shear stresses and strains for each salt specimen (Table5.2)

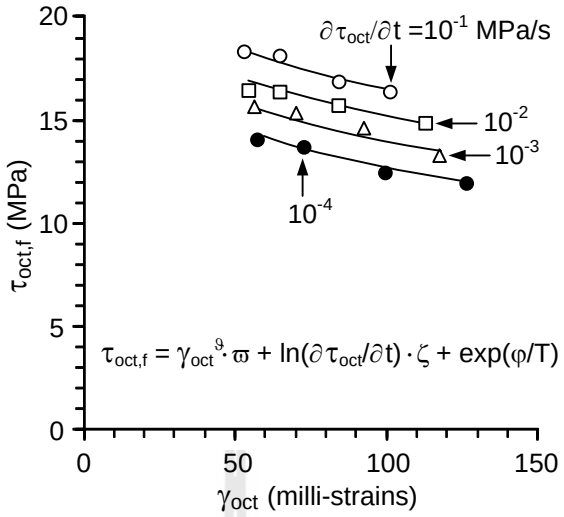

Figure 5.9 Octahedral shear stress at failure as a function of octahedral shear strain for various octahedral shear stress rates.

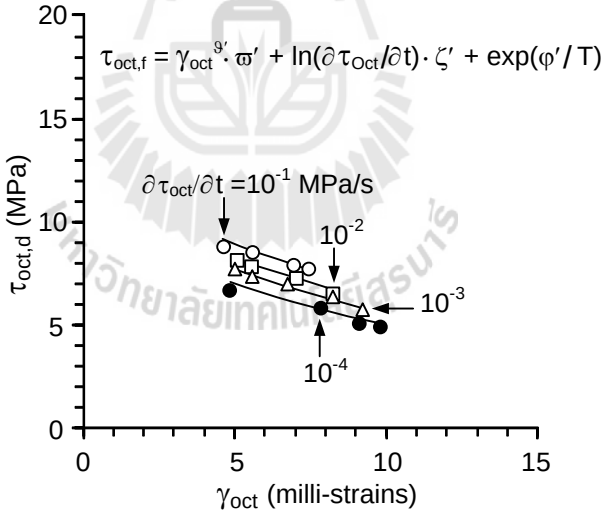

Figure 5.10 Octahedral shear stress at dilation as a function of octahedral shear strain for various octahedral shear stress rates.

using the following relations (Jaeger et al., 2007):

$$W_d = (3/2)\cdot\tau_{oct,f}\cdot\gamma_{oct,f} \quad (5.19)$$

$$W_{d,d} = (3/2)\cdot\tau_{oct,d}\cdot\gamma_{oct,d} \quad (5.20)$$

where $\tau_{oct,f}$, $\tau_{oct,d}$ are octahedral shear stress at failure and at dilation, $\gamma_{oct,f}$, $\gamma_{oct,d}$ are octahedral shear strain at failure and at dilation.

The distortion strain energy at dilation ($W_{d,d}$) is presented as a function of the mean strain energy density at dilation ($W_{m,d}$) which can be calculated from $\sigma_{m,d}$ and $\varepsilon_{m,d}$ as follows:

$$W_{m,d} = (3/2)\cdot\sigma_{m,d}\cdot\varepsilon_{m,d} \quad (5.21)$$

Figure 5.11 shows a linear relation between $W_{d,d}$ and $W_{m,d}$ which can be represented by:

$$W_{d,d} = 1.370\cdot W_{m,d} - 0.004 \quad \text{(MPa)} \quad (5.22)$$

The proposed criterion considers both stress and strain at dilation, and hence isolating the effect of stress rate and temperature. If the salt temperature is known its strength at dilation can be determined from equation (5.22) regardless the loading rate.

Table 5.2 Strain energy density at failure and at dilation under various loading rates and temperatures.

Temperature (Kelvin)	$\partial\tau_{oct}/\partial t$ (MPa/s)	W_d (MPa)	W_m (MPa)	$W_{d,d}$ (MPa)	$W_{m,d}$ (MPa)
273	0.1	2.47	0.51	0.40	0.29
	0.01	2.51	0.49	0.40	0.29
	0.001	2.34	0.51	0.37	0.27
	0.0001	2.24	0.61	0.36	0.27
303	0.1	2.04	0.40	0.33	0.26
	0.01	1.99	0.41	0.32	0.24
	0.001	2.05	0.41	0.33	0.23
	0.0001	1.82	0.37	0.29	0.21
343	0.1	1.73	0.40	0.28	0.21
	0.01	1.55	0.39	0.25	0.19
	0.001	1.61	0.40	0.26	0.19
	0.0001	1.50	0.37	0.24	0.18
373	0.1	1.45	0.28	0.23	0.17
	0.01	1.35	0.30	0.22	0.16
	0.001	1.32	0.29	0.21	0.16
	0.0001	1.20	0.30	0.19	0.14

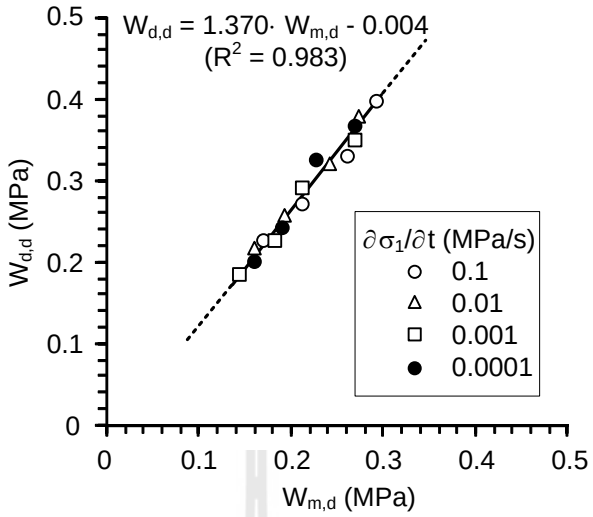

Figure 5.11 Distortional strain energy at dilation ($W_{d,d}$) as a function of mean strain energy at dilation ($W_{m,d}$).

CHAPTER VI

COMPUTER SIMULATIONS

6.1 Objective

This section describes a result of finite difference analysis using FLAC (Itasca, 1992) to simulations of the single isolate cavern in axial symmetry. The principal stresses and strains induced in the surrounding salt under various air withdrawal rates are calculated and compared against the criteria. They are used to determine the safe maximum withdrawal rate of compressed-air energy storage (CAES) cavern in the Maha Sarakham salt formation.

6.2 Numerical simulation

Finite difference analyses (FLAC 4.0) are performed to determine the stresses and strains at the boundaries of CAES caverns for various reduction rates of the internal pressures. Figure 6.1 shows the mesh modal representing the cavern from the ground surface to the depth of 1000 m. The caverns are up-right cylinder with the casing shoe (cavern top) at 300, 400 and 500 m. The cavern diameter and height are 50 m and 300 m.

The in-situ stress is assumed to be hydrostatic. Before cavern development the salt stress at the casing shoe depth (σ_{cs}) is calculates as 6.5, 8.6 and 10.8 MPa for casing shoe depth 300, 400 and 500 m, respectively. The maximum cavern pressure defined as $0.9\sigma_{cs}$. Two cases with different minimum cavern pressure that are

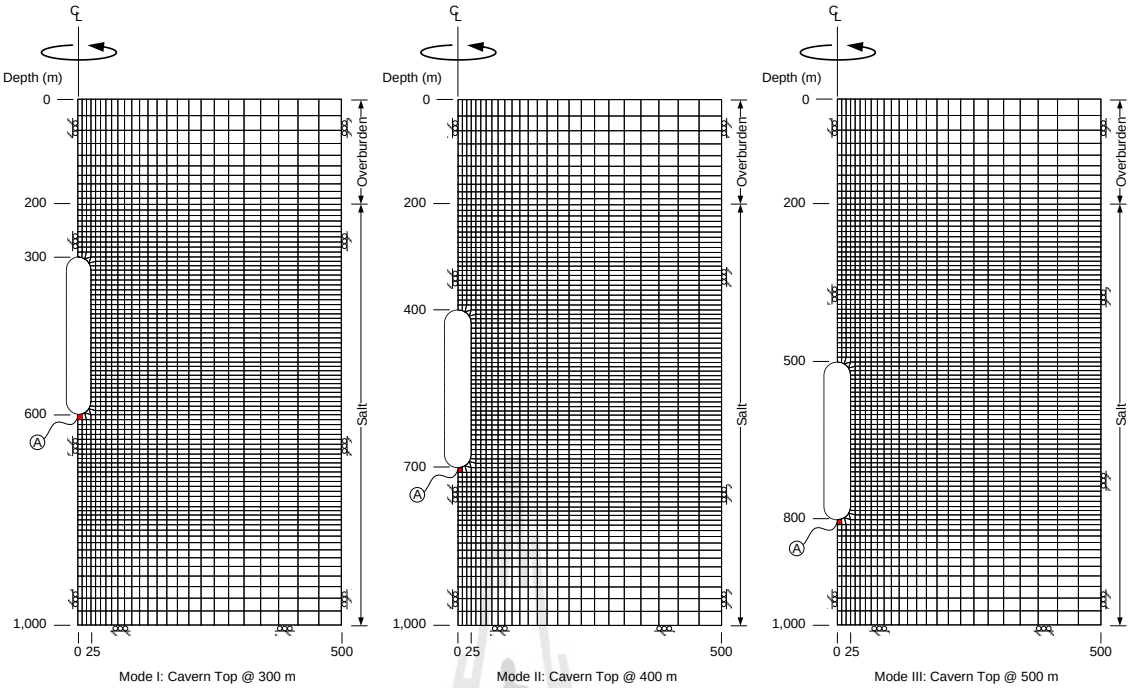

Figure 6.1 Finite difference mesh developed for FLAC simulation of CAES cavern.

commonly used for the saltstorage caverns are studied: $0.1\sigma_{cs}$, $0.2\sigma_{cs}$. Each case simulated for four different rates of cavern pressure withdrawal. The equivalent pressure schemes are calculated by assuming that the air injection and retrieval periods are equal.

The Maha Sarakham salt is assumed to behave as a Burgers material. The Burgers constitutive equation is a built-in program in FLAC (Itasca, 1992); as follows:

$$\gamma_{oct} = \tau_{oct}\left[\left(\frac{t}{\eta_1}+\frac{1}{E_1}+\frac{\eta_1}{\eta_2 E_2}\right)-\left(\frac{\eta_1}{\eta_2 E_2}\exp\left(\frac{-E_2 t}{\eta_2}\right)\right)\right] \qquad (6.1)$$

where τ_{oct} is octahedral shear stresses (MPa), t is time (day), E_1 is elastic modulus

(GPa), E_2 is spring constant in visco-elastic phase (GPa), η_1 is visco-plastic coefficient in steady-state phase (GPa.day) and η_2 is visco-elastic coefficient in transient phase (GPa.day).

Figure 6.2 show the modular components of the Burgers model. The Burgers parameters for the Maha Sarakham salt are obtained from the calibration results of creep tests under temperature of the same salt. The parameters are given in Table 6.1.

Tables 6.2 and 6.3 summarize the simulation results for two case in terms of the mean stresses and strains, octahedral shear stresses and strains and distortional and mean strain energy at the bottom of the cavern (point A – Figure 6.1). For all case the magnitudes of the mean and shear stresses and strains decrease with the withdrawal rate. The octahedral shear stresses and strains for the minimum pressure 10% are slightly greatly than those for the 20%.

6.3 Factor of safety calculation

For a conservative design the surrounding salt is not allowed to dilate during the withdrawal period. This is to ensure the long-term stability of the storage cavern under loading. As a result the three dilation criteria are used here to calculate the factor of safety (FS) of the salt at the bottom of the cavern. These include $\tau_{oct,d}$ - $\partial\tau_{oct}/\partial t$ criterion (equation (5.15)), $\tau_{oct,d}$ - $\gamma_{oct,d}$ criterion (equation (5.17)) and $W_{d,d}$ – $W_{m,d}$ criterion (equation (5.21)).

The FS calculation methods and results for all pressure schemes are shown in Tables 6.4 – 6.6. The three criteria give difference FS values. The $\tau_{oct,d}$ - $\gamma_{oct,d}$ criterion tend to give the largest FS values for all cases. This criterion does not consider the mean stresses and strains induced around the cavern. The FS values

obtained from applying the $\tau_{oct,d}$ - $\partial\tau_{oct}/\partial t$ criterion are between those obtained from the other two criteria. This criterion does not consider the mean stresses and strains induced around the cavern. The simulation results indicate that the safety withdrawal rates are increase with decreasing withdrawal rate. As shown in Tables 6.4 – 6.6, for all criteria the factors of safety calculated for 20% minimum pressure are greater than those for the 10%.

The $W_{d,d} - W_{m,d}$ criterion gives the most conservative results. It shows the FS values lower than 1.0 for the withdrawal rates of 1 cycle/day and 15 cycles/month. This criterion is perhaps the most appropriate for use in the design of the withdrawal rate because it incorporates both shear and mean stresses and strains.

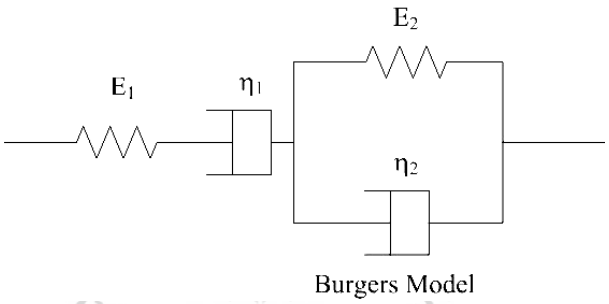

Figure 6.2 Modular components of the Burgers model.

Table 6.1 Material parameters used in FLAC simulations.

Parameters	Symbols	Units	Values
Elastic modulus	E_1	GPa	1.183
Spring constant in visco-elastic phase	E_2	GPa	3.109
visco-plastic coefficient in steady-state phase	η_1	GPa.day	64.593
visco-elastic coefficient in transient phase	η_2	GPa.day	0.647

Table 6.2 Stresses and strains at cavern bottom from FLAC simulations for $0.1\sigma_{cs}$ at 300, 400 and 500 m of casing shoe depth.

Depth (m)	Pressure scheme	Pressure reduction duration (day)	Pressure withdrawal rate (MPa/day)	σ_m (MPa)	ε_m ($\times 10^{-3}$)	τ_{oct} (MPa)	γ_{oct} ($\times 10^{-3}$)	W_m (MPa)	W_d (MPa)
300	1cycle/day	0.5	10.4	14.1	4.592	5.0	71.8	0.097	0.543
	15 cycles/month	1	5.2	13.6	3.492	4.6	48.8	0.071	0.334
	1 cycle/month	15	0.4	13.3	2.247	2.1	16.8	0.045	0.053
	6 cycles/year	30	0.2	13.1	1.204	2.4	6.3	0.024	0.022
400	1cycle/day	0.5	13.8	16.3	5.052	5.4	70.1	0.124	0.572
	15 cycles/month	1	6.9	15.8	5.202	4.0	62.2	0.123	0.369
	1 cycle/month	15	0.5	15.1	4.834	2.7	30.2	0.109	0.122
	6 cycles/year	30	0.2	14.8	4.275	2.5	26.6	0.095	0.098
500	1 cycle/day	0.5	17.2	18.5	6.060	6.2	68.1	0.169	0.631
	15 cycles/month	1	8.6	18.1	5.885	4.5	61.6	0.160	0.419
	1 cycle/month	15	0.6	17.3	5.404	3.1	40.3	0.140	0.186
	6 cycles/year	30	0.3	16.8	5.375	2.8	38.0	0.135	0.159

Table 6.3 Stresses and strains at cavern bottom from FLAC simulations for $0.2\sigma_{cs}$ at 300, 400 and 500 m of casing shoe depth.

Depth (m)	Pressure scheme	Pressure reduction duration (day)	Pressure withdrawal rate (MPa/day)	σ_m (MPa)	ε_m ($\times 10^{-3}$)	τ_{oct} (MPa)	γ_{oct} ($\times 10^{-3}$)	W_m (MPa)	W_d (MPa)
300	1cycle/day	0.5	9.0	15.1	5.155	5.0	71.2	0.117	0.535
	15cycles/month	1	4.5	14.7	4.572	3.6	41.6	0.101	0.222
	1 cycle/month	15	0.3	14.2	3.469	2.2	27.1	0.074	0.089
	6 cycles/year	30	0.2	14.1	2.221	2.1	16.0	0.047	0.049
400	1cycle/day	0.5	12.2	16.5	4.310	5.4	64.8	0.107	0.525
	15cycles/month	1	6.1	14.8	4.044	3.8	62.2	0.090	0.354
	1 cycle/month	15	0.4	14.5	3.819	2.6	27.5	0.083	0.106
	6 cycles/year	30	0.2	14.5	3.229	2.4	21.6	0.070	0.078
500	1 cycle/day	0.5	15.0	17.7	4.978	5.9	60.8	0.132	0.538
	15cycles/month	1	7.5	16.7	4.939	4.4	47.1	0.123	0.312
	1 cycle/month	15	0.5	15.7	4.379	2.9	27.2	0.103	0.120
	6 cycles/year	30	0.3	15.7	4.366	2.5	29.0	0.103	0.107

Table 6.4 Factor of safety at cavern bottom based on $\tau_{oct,d}$ - $\partial\tau_{oct}/\partial t$ criterion.

Depth (m)	Pressure scheme	$\tau_{oct,d} = \ln(\partial\tau_{oct}/\partial t)\cdot$ ɜ′ + exp(η′/T) + ι′ (MPa)	
		Factor of Safety ($FS = \tau_{oct,d}/\tau_{oct}$)	
		$0.2\sigma_{cs}$	$0.1\sigma_{cs}$
300	1 cycle/day	0.88	0.87
	15cycles/month	1.16	0.91
	1 cycle/month	1.40	1.45
	6 cycles/year	1.36	1.18
400	1 cycle/day	0.84	0.83
	15cycles/month	1.12	1.07
	1 cycle/month	1.23	1.18
	6 cycles/year	1.20	1.18
500	1 cycle/day	0.78	0.74
	15cycles/month	0.77	0.75
	1 cycle/month	1.11	1.06
	6 cycles/year	1.22	1.07

Table 6.5 Factor of safety at cavern bottom based on $\tau_{oct,d}$ - $\gamma_{oct,d}$ criterion.

Depth (m)	Pressure scheme	$\tau_{oct,d} = \varpi' \cdot \gamma_{oct,d}^{\ g'} + \ln(\partial\tau_{oct}/\partial t) \cdot \zeta' + \exp(\varphi'/T)$ (MPa)	
		Factor of Safety ($FS = \tau_{oct,d}/\tau_{oct}$)	
		$0.2\sigma_{cs}$	$0.1\sigma_{cs}$
300	1 cycle/day	0.47	0.46
	15cycles/month	0.71	0.55
	1 cycle/month	1.44	1.49
	6 cycles/year	1.62	1.41
400	1 cycle/day	0.42	0.42
	15cycles/month	0.64	0.62
	1 cycle/month	1.19	1.15
	6 cycles/year	1.34	1.32
500	1 cycle/day	0.38	0.36
	15cycles/month	0.66	0.65
	1 cycle/month	1.03	0.98
	6 cycles/year	1.30	1.14

Table 6.6 Factor of safety at cavern bottom based on $W_{d,d} - W_{m,d}$ criterion.

Depth (m)	Pressure scheme	$W_{d,d} = 1.37W_{m,d} - 0.004$ (MPa)				Factor of Safety ($FS = W_{d,d}/ W_d$)	
		$0.2\sigma_{cs}$		$0.1\sigma_{cs}$		$0.2\sigma_{cs}$	$0.1\sigma_{cs}$
		$W_{m,d}$ (MPa)	$W_{d,d}$ (MPa)	$W_{m,d}$ (MPa)	$W_{d,d}$ (MPa)		
300	1 cycle/day	0.117	0.156	0.097	0.129	0.29	0.24
	15cycles/month	0.101	0.134	0.071	0.094	0.60	0.28
	1 cycle/month	0.074	0.097	0.045	0.058	1.09	1.08
	6 cycles/year	0.047	0.061	0.024	0.028	1.23	1.27
400	1 cycle/day	0.107	0.142	0.124	0.165	0.27	0.29
	15cycles/month	0.090	0.119	0.123	0.165	0.34	0.45
	1 cycle/month	0.083	0.110	0.109	0.146	1.04	1.20
	6 cycles/year	0.070	0.092	0.095	0.126	1.18	1.28
500	1 cycle/day	0.132	0.177	0.169	0.227	0.33	0.36
	15cycles/month	0.123	0.165	0.160	0.215	0.53	0.51
	1 cycle/month	0.103	0.137	0.140	0.188	1.15	1.01
	6 cycles/year	0.103	0.137	0.135	0.181	1.28	1.14

CHAPTER VII

DISCUSSIONS, CONCLUSIONS AND RECOMMENDATIONS FOR FUTURE STUDIES

7.1 Discussions and conclusions

The effect of loading rate on compressive strength and deformability are determined for cylindrical salt specimens obtained from Maha Sarakham salt. The compression load frame applies axial stresses at constants rates of 0.0001, 0.001, 0.01 and 0.1 MPa/s. The testing temperatures are maintained constant of 273, 303, 343 and 373 Kelvin.

The failure stresses increase with the loading rates, these agree with the experimental results on rock salt performed by (Fuenkajorn et al., 2012; Dubey and Gairola, 2005). The testing is assumed to be under isothermal conditions (constant temperature with time during loading). The decreases of the compressive strengths with increasing temperatures agree with the experimental results (Sriapai et al.,2012; Vosteen and Schellschmidt, 2003; Adhikary, 2010). Their results indicated that the compressive strengths of the salt decrease with increasing temperatures. The decrease of the salt strength as the temperature increases suggests that the applied thermal energy before the mechanical testing makes the salt weaker, and more plastic, failing at lower stress and higher strain with lower elastic moduli. The salt elastic modulus varies from 11 to 29 GPa. The Poisson's ratio from 0.31 to 0.42, and tend to be independent of the loading rate and temperature. Under the range of the tested

parameters the salt shows non-linear behavior particularly under low loading rates and high temperatures. The exponential creep law represents the salt creep under compression and isothermal condition. It can well describe the creep strain for all tested temperatures.

Several forms of the strength and dilation criteria have been derived. The $\tau_{oct,f}$ - $\partial\tau_{oct}/\partial t$ and $\tau_{oct,d}$ - $\partial\tau_{oct}/\partial t$ criteria are the simplest. They do not consider the induced strains, but incorporate the effects of the shear rate and temperature into their formulation. The shear strain induced at dilation and failure are added into the formulation of the $\tau_{oct,f}$ - $\gamma_{oct,f}$ and $\tau_{oct,d}$ - $\gamma_{oct,d}$ criteria to implicitly consider the rate and temperature effects.

Assuming that the rock salt is non-linearly elastic before failure, the distortional strain energy ($W_{d,d}$) at dilation can be calculated as a function of mean strain energy ($W_{m,d}$). For given $W_{m,d}$ the $W_{d,d}$ decreases with increasing temperature. The strain energy criterion agrees well with the strength results from different temperature.

The criteria proposed above can be used in the calculation of factor of safety of salt cavern. The Burgers model has been used in the FLAC simulation to determine the stresses and strains around the cavern. The results are compared against criteria developed above for calculate the maximum withdrawal rate of the compressed-air storage cavern.

7.2 Recommendations for future studies

The uncertainties and adequacies of the research investigation and results discussed above lead to the recommendations for further studies. The test specimens

here are relatively small. Testing on larger specimens is desirable to confirm the research findings. Verification of the compression test proposed concept should be tested under a wider range of salt from other sources. The effect of cyclic thermal and mechanical loading should be assessed. More testing is needed to confirm the applicability and limitations of the proposed, such as true triaxial creep test, multi-step triaxial loading, and triaxial cyclic loading test.

REFERENCES

Adhikary, S. (2010). **Temperature effect on the rock salt instant strength characteristics**, M.S. Thesis, Delft University of Technology, Netherlands. 48 p.

Albertin, M., Julien, M. R., Servant, S. and Gill, E. (1999). A rate-dependent model for the ductile behavior of salt rock. **Canadian Geotechnical Journal** 36: 660-674.

Archeeploha, S. and Fuenkajorn, K. (2012). Thermal effects on strength and deformability of Maha Sarakham salt. In **Proceedings of the Second Southern Hemisphere Symposium SHIRMS 2012** (pp. 47-61). May 15-17, Sun City, Pilansberg, South Africa.

Backers, T., Fardinb, N., Dresena, G. and Stephanssona, O. (2003). Effect of loading rate on Mode I fracture toughness, roughness and micromechanics of sandstone. **International Journal of Rock Mechanics and Mining Sciences** 40: 425-433.

Charpentier, J-P. (1984). Creep of rock salt elevated temperature. In **Proceedings of the Second Conference on the Mechanics Behavior of Salt** (pp. 131-136). Clausthal, Germany: Trans Tech Publications.

Cristescu, N. D and Hunsche, U. (1998). Time effects in Rock Mechanics. John Wiley & Sons, New York.

Dubey, R. K. and Gairola, V. K. (2005). Influence of stress rate on rheology-An experimental study on rock salt of Simla Himalaya, India. **Geotechnical and Geological Engineering** 23: 757-772.

Dwivedi, R. D., Goel, R. K., Prasada, V. V. R. and Sinhab, A. (2008). Thermo-mechanical properties of Indian and other granites. **International Journal of Rock Mechanics and Mining Sciences** 45: 303-315.

Farmer, I. W. (1983). **Engineering Behavior of Rock Second Edition**, Chapman and Hall, London.

Fuenkajorn, K. and Kenkhunthod, N. (2010). Influence of loading rate on deformability and compressive strength of three Thai sandstones. **Geotechnical and Geological Engineering** 28(5): 707-715.

Fuenkajorn, K., Sriapai, T. and Samsri, P. (2012). Effects of loading rate on strength and deformability of Maha Sarakham salt. **Engineering Geology** 135-136: 10-23.

Hamami, M. (1999). Simulataneous effect of loading rate and confining pressure on the deviator evolution in rock salt. **International Journal of Rock Mechanics and Mining Sciences** 36: 827-831.

Hamami, M., Tijani, S. M. and Vouille, G. (1996). A methodology for the identification of rock salt behavior using multi-steps creep tests. In **Proceedings of the Third Conference on the Mechanical Behavior of Salt** (pp. 53-66). Clausthal-Zellerfeld: Trans Tech Publications.

Hansen, F. D. (1984). Physical and mechanical variability of natural rock salt. In **Proceedings of the Second Conference on the Mechanical Behavior of Salt** (pp. 23-39). Clausthal-Zellerfeld: Trans Tech Publications.

Hashiba, K., Okubo, S., and Fukui, K. (2006). A new testing method for investigating the loading rate dependency of peak and residual rock strength. **International Journal of Rock Mechanics and Mining Sciences** 43: 894–904.

Huang, B. and Liu, J. (2013). The effect of loading rate on the behavior of samples composed of coal and rock. **International Journal of Rock Mechanics and Mining Sciences** 61: 23-30.

Itasca. (1992). **User Manual for FLAC-Fast Langrangian Analysis of Continua, Version 4.0.** Itasca Consulting Group Inc., Minneapolis, Minnesota.

Jaeger, J. C., Cook, N. G. W. and Zimmerman, R. W. (2007). **Fundamentals of Rock Mechanics Fourth Edition** (500 pp.). Blackwell publishing, Oxford.

Jeremic, K. L. (1994). **Rock Mechanics in Salt Mining** (530 pp.). Rotherdam: A. A. Balkema.

Khathipphathee, T. and Fuenkajorn, K. (2013). Performance assessment of Maha Sarakham salt for CO_2 storage. In **Proceedings of the Fourth Thailand Symposium on Rock Mechanics** (pp. 111-119). January 24-25, Im Poo Hill Resort, Nakhon Ratchasima, Thailand.

Kumar, A. (1968). The effect of stress rate and temperature on the strength of basalt and granite. **Geophysics** 33(3): 501-510.

Lajtai, E. Z., Duncan, E. J. S. and Carter, B. J. (1991). The effect of strain rate on rock strength. **Rock Mechanics and Rock Engineering** 24: 99-109.

Langer, M. (1984). The Rheological behavior of rock salt, Mechanical behavior of salt I. In **Proceedings of the First Conference on the Mechanical Behavior of Salt** (pp. 201-240). Clausthal-Zellerfeld, Germany: Trans Tech Publications.

Liang, W. G., Zhao, Y. S., Xu, S. G. and Dusseault, M. B. (2011). Effect of strain rate on the mechanical properties of salt rock. **International Journal of Rock Mechanics and Mining Sciences** 48: 161-167.

Ma, L. and Daemen, J. J. K. (2006). Strain rate dependent strength and stress-strain characteristics of a welded tuff. **Bulletin of Engineering Geology and the Environment** 65(3): 221-230.

Okatov, R. P., Nizametdinov, F. K., Tsai, B. N. and Bondarenko, T. T. (2003). Time and temperature factors in construction of rock strength criteria. **Journal of Mining Science** 39(2): 139-142.

Okubo, S., Fukui, K. and Qingxin, Q. (2006). Uniaxial compression and tension tests of anthracite and loading rate dependence of peak strength. **International Journal of Coal Geology** 68: 196-204.

Pudewills, A. (1995). **Thermal Simulation of Drift Emplacement: Temperature Analyses.** Topical Report, Forschungszentrum Karlsruhe.

Pudewills, A. and DrostePapp, J. (2003). Numerical modeling of the thermomechanical behavior of a large-scale underground experiment. **Computers & Structures** 81: 911-918.

Ray, S. K., Srakar, M. and Singh, T. N. (1999). Effect of cyclic loading and strain rate on the mechanical behaviour of sandstone. **International Journal of Rock Mechanics and Mining Sciences** 36: 543-549.

Sangha, C. M. and Dhir, R. K. (1972). Influence of time on the strength, deformation and fracture properties of a lower Devonian sandstone. **International Journal of Rock Mechanics and Mining Sciences** 9: 343-354.

Sheinin, V. I. and Blokhin, D. I. (2012). Features of thermomechanical effects in rock salt samples under uniaxial compression. **Journal of Mining Science** 48(1): 39-45.

Shimada, M. and Liu, J. (2000). Temperature dependence of strength of rock under high confining pressure. **Annuals Disaster Prevention Research Institute** 43B-1: 75-84.

Sriapai, T., Walsri, C. and Fuenkajorn, K. (2012). Effect of temperature on compressive and tensile strength of salt. **Scienceasia** 38: 166-174.

Tabakh, M. E., Ultha-Aroon, C. and Schreiber, B. C. (1999). Sedimentology of the Cretaceous Maha Sarakham evaporates in the Khorat plateau of northeastern Thailand. **Sedimentary Geology** 123: 31-62.

Vosteen, H. and Schellschmidt, R. (2003). Influence of temperature on thermal conductivity, thermal capacity and thermal diffusivity for different types of rock. **Physics and Chemistry of the Earth** 28: 499-509.

Warren, J. (1999). **Evaporites: Their Evolution and Economics**. Blackwell Science, Oxford. 438 p.

Wendai, L. (2000). Regression analysis, linear regression and probit regression In 13 chapters. SPSS for Windows: statistical analysis. Publishing House of Electronic Industry, Beijing.

Yanan, G., Feng, G., Zhizhen, Z. and Tao, Z. (2010). Visco – elastic model of deep underground rock affect by temperature and humidty. **Mining Science and Technology** 20: 183-187.

Yang, C. and Daemen, J. J. K. (1997). Temperature effects on creep of tuff and its time-dependent damage analysis. **International Journal of Rock Mechanics and Mining Sciences** 34(3-4): 383-395.

Yang, C., Daemen, J. J. K. and Yin, J. H. (1999). Experimental investigation of creep behavior of salt rock. **International Journal of Rock Mechanics and Mining Sciences** 36: 233-242.

APPENDIX A

PUBLICATION

List of Publication

Sartkaew, S. and Fuenkajorn, K. (2013). Effects of stress rate on uniaxial compressive strength of rock salt under 0-100°C. In **Proceedings of the 11th International Conference on Mining, Materials and Petroleum Engineering, the 7th International Conference on Earth Resources Technology, ASEAN Forum on Clean Coal Technology** (pp. 13-20). November 11-13, Centara Duangtawan Hotel, Chiang Mai, Thailand, pp. 13-20.

ASEAN++ 2013 Moving Forward
The 11th International Conference on Mining, Materials and Petroleum Engineering
The 7th International Conference on Earth Resources Technology
ASEAN Forum on Clean Coal Technology
November 11-13, 2013, Chiang Mai, Thailand

Paper ID 100

Effects of Stress Rate on Uniaxial Compressive Strength of Rock Salt under 0-100°C.

S. Sartkaew[1]*, K. Fuenkajorn[2]
[1]*Graduate Student, Geomechanics Reserarch Unit, Suranaree University of Technology, Thailand*
[2]*Associate Professor, Geomechanics Reserarch Unit, Suranaree University of Technology, Thailand*
**e-mail: suratwadee-s@hotmail.com*

ABSTRACT

Uniaxial compression test have been performed to assess the effects of loading rate on compressive strength and deformability of the Maha Sarakham salt under temperatures ranging from 273 to 373 Kelvin (0-100°C). The variation of the octahedral shear strength with the stress rates and temperatures can be described by logarithmic relations. The distortion strain energy criterion is proposed to describe the salt strength under varied stress rates and temperatures. The criterion can be used to determine the stability of salt around compressed-air energy storage caverns, where the loading rates and temperatures are continuously varied during air injection and retrieval periods.

KEYWORDS: *Rock salt / Loading rate / Thermal effect / Strain energy*

1. INTRODUCTION

The effects of loading rate on the compressive strength and deformability of intact rocks have long been recognized [1-4]. For rock salt such effects have been studied by various researchers [5-8]. It has been found that the salt strength increases with the applied stress and strain rates. The rock strength and elastic properties have been known to decrease as the temperature increases [9]. Several formulations have been proposed to describe the temperature-dependent behavior of rock salt [9-11]. Such knowledge is necessary for stability analysis and design of the salt storage caverns. During injection period the storage caverns may subject to temperatures as high as 140°C (414 K), depending on the injection rate and the maximum storage volume and pressure [9].

The objective of this study is to experimentally assess the influence of loading rate on the compressive strength and deformability of rock salt under constant temperatures of 273, 303, 343 and 373 K. This selected range of temperatures covers those likely occur around salt storage caverns under operation. Uniaxial compression test have been performed on the Maha Sarakham salt under loading rates from 0.0001 to 0.1 MPa/s. The strain energy density criterion is proposed to describe the salt strength as affected by the loading rates and temperatures.

2. SALT SPECIMENS

The salt specimens are prepared from 47 mm salt cores drilled from depths ranging between 270 and 330 m by Siam Submanee Co., Ltd. in the northeast of Thailand. The salt cores belong to the Lower salt member of the Maha Sarakham formation. Tabakh et al. [12] describe the origin and geologic sequence of the Maha Sarakham salt. The drill cores were dry-cut to obtain cylindrical shaped specimens with nominal dimensions of 47 mm diameter and 118 mm length.

To test the salt specimens under elevated temperatures, they are wrapped with heating tape, foil and insulator for 24 hours before testing. A digital temperature regulator is used to maintain constant temperature to the specimens. The low temperature specimens are cooled in a cooling system during the test. As a result the specimen temperatures are assumed to be uniform and constant with time during the mechanical testing i.e., isothermal condition.

3. TEST METHOD

The salt specimen is placed in a compression machine and loaded axially until failure (Fig. 1). The applied stress rates are constant at of 0.0001, 0.001, 0.01 and 0.1 MPa/s. For the low temperature testing the loading frame is placed inside a cooling system (Fig. 2). The salt specimen is cooled for 48 hours before starts loading. It can cool the salt specimens down to 273 K. For the high temperature testing a heating tape with temperature regulator are used to apply constant elevated temperatures while loading (Fig. 3). Photographs are taken of the failed specimens.

ASEAN++ 2013 Moving Forward
The 11th International Conference on Mining, Materials and Petroleum Engineering
The 7th International Conference on Earth Resources Technology
ASEAN Forum on Clean Coal Technology
November 11-13, 2013, Chiang Mai, Thailand

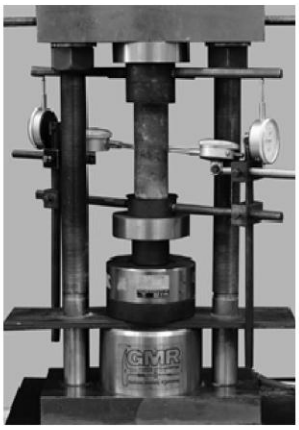

Fig. 1 Salt specimen placed in a compression machine under room temperature (about 303 K).

Fig. 2 Salt specimen placed in the consolidation load frame and inside the cooling system for low temperature at 273 K.

4. TEST RESULTS

Fig. 4 shows the stress-strain curves monitored from some of the salt specimens under different stress rates and temperatures. Tab. 1 gives the test results. The specimens tend to show nonlinear behavior, particularly under high temperatures. All post-test specimens show shear failure mode (Fig. 5). Under the same loading rate ($\partial\sigma_1/\partial t$), the compressive strength (σ_c) decreases with increasing specimen temperatures. The mean stresses (σ_m) and strains (ε_m) and octahedral shear stresses ($\tau_{oct,f}$) and shear strains ($\gamma_{oct,f}$) at failure are determined using the following relations [13]:

$$\sigma_m = (\sigma_1+\sigma_2+\sigma_3)/3 \quad (1)$$

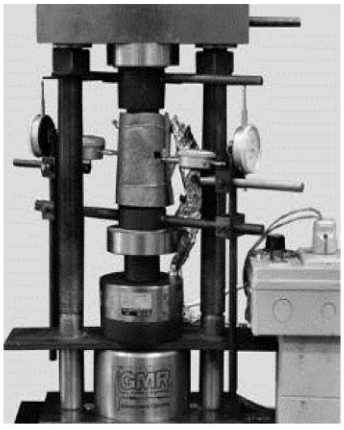

Fig. 3 Salt specimen wrapped with the heating tape and insulator for high temperature testing at 343 and 373 K.

$$\varepsilon_m = (\varepsilon_1+\varepsilon_2+\varepsilon_3)/3 \quad (2)$$

$$\tau_{octf} = (1/3)\left[(\sigma_1-\sigma_2)^2+(\sigma_1-\sigma_3)^2+(\sigma_2-\sigma_3)^2\right]^{1/2} \quad (3)$$

$$\gamma_{oct,f} = (1/3)\left[(\varepsilon_1-\varepsilon_2)^2+(\varepsilon_1-\varepsilon_3)^2+(\varepsilon_2-\varepsilon_3)^2\right]^{1/2} \quad (4)$$

where σ_1, σ_2 and σ_3 are the major, intermediate and minor principal stresses at failure.

The applied octahedral shear stresses are plotted as a function of octahedral shear strain in Fig. 6. The shear stress-strain relations are nonlinear, particularly under low loading rates and high temperatures. Higher shear strengths and lower shear strains are observed under low stress rates and high temperatures.

The variation of the shear strengths can be observed from the τ_{oct} - σ_m diagram, as shown in Fig. 7. The linear relation between the octahedral shear strength and the mean stress at failure and can be best represented by:

$$\tau_{oct,f} = 1.412\cdot\sigma_m + 0.022 \quad \text{MPa} \quad (5)$$

5. SALT DEFORMATIONS

The total compressive strain is divided here into two parts; elastic strain (linear and recoverable strain) and plastic creep strain (time-dependent and nonrecoverable strain):

$$\varepsilon_c = \varepsilon_c^e + \varepsilon_c^c \quad (6)$$

where ε_c is the total compressive strain, ε_c^e is elastic strain, ε_c^c is plastic creep strains.

ASEAN++ 2013 Moving Forward
The 11th International Conference on Mining, Materials and Petroleum Engineering
The 7th International Conference on Earth Resources Technology
ASEAN Forum on Clean Coal Technology
November 11-13, 2013, Chiang Mai, Thailand

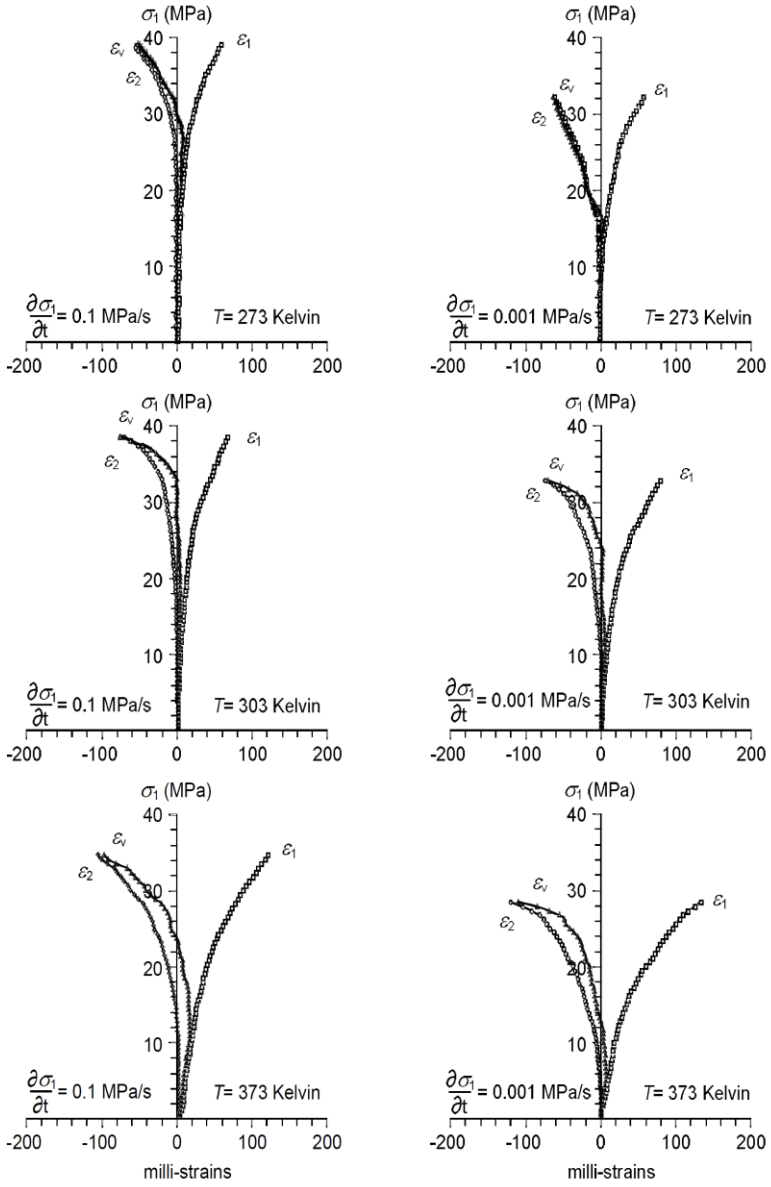

Fig. 4 Stress-strain curves obtained from some salt specimens with different loading rates ($\partial\sigma_1/\partial t$) and temperatures ($T$).

The elastic strain can be calculated from the current stress state using classical elastic theory [13]:

$$\varepsilon_c^e = \frac{\sigma_c}{E} \tag{7}$$

where σ_c is the compressive stress, E is the elastic modulus. The exponential creep law is used to describe time-dependent strain of the salt [14]:

$$\varepsilon_c^c = \alpha \cdot \sigma_c^{\beta} \cdot t^{\kappa} \cdot exp\left(\frac{-\lambda}{T}\right) \tag{8}$$

ASEAN++ 2013 Moving Forward
The 11th International Conference on Mining, Materials and Petroleum Engineering
The 7th International Conference on Earth Resources Technology
ASEAN Forum on Clean Coal Technology
November 11-13, 2013, Chiang Mai, Thailand

Tab. 1 Salt strengths under various loading rates and temperatures.

Average Temperature (K)	Stress rate (MPa/s)	Compressive Strength (MPa)	Mean Stress (MPa)
273	0.1	38.79	12.93
	0.01	34.94	11.65
	0.001	33.22	11.07
	0.0001	29.78	9.93
303	0.1	37.23	12.41
	0.01	34.56	11.52
	0.001	32.59	10.86
	0.0001	29.19	9.73
343	0.1	35.78	11.93
	0.01	33.51	11.17
	0.001	29.69	9.90
	0.0001	26.58	8.86
373	0.1	34.60	11.53
	0.01	31.51	10.50
	0.001	28.11	9.37
	0.0001	25.16	8.39

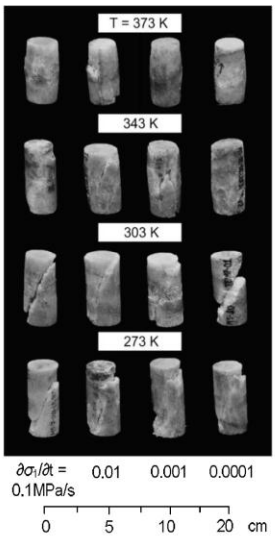

Fig. 5 Post-test specimens from uniaxial compressive strength testing under different loading rates ($\partial\sigma_1/\partial t$) and temperatures ($T$).

where α, β, κ and λ are empirical constants and T is constant temperature in Kelvin. Substituting equations (7) and (8) into (6) we obtain:

$$\varepsilon_c = \frac{\sigma_c}{E} + \alpha \cdot \sigma_c^{\beta} \cdot t^{\kappa} \cdot exp\left(\frac{-\lambda}{T}\right) \quad (9)$$

Similarly the creep parameters can also be derived in the forms of the octahedral shear strain:

$$\gamma_{oct} = \frac{\tau_{oct}}{2G} + \alpha \cdot \tau_{oct}^{\beta} \cdot t^{\kappa} \cdot exp(-\lambda/T) \quad (10)$$

where γ_{oct} is the octahedral shear strain, τ_{oct} is the octahedral shear stress, G is shear modulus, α is stress constant, β is stress exponent, T is temperature (Kelvin), t is time, κ is time exponent and λ is temperature constant.

For the stress-rate controlled condition the octahedral shear stress at any loading time (t) can be expressed as:

$$\gamma_{oct}(t) = \frac{\dot{\tau}_{oct} \cdot t}{2G} + \alpha \cdot exp\left(\frac{-\lambda}{T}\right) \cdot \dot{\tau}_{oct}^{\beta} \cdot t^{\beta+\kappa} \quad (11)$$

Assuming that the salt elasticity varies linear with temperature [9]:

$$G = \psi \cdot T + G_0 \quad (12)$$

where G_0 is shear modulus at zero Kelvin and ψ is the empirical constant. Substitute equation (12) into (11) we obtain:

$$\gamma_{oct}(t) = \frac{\dot{\tau}_{oct} \cdot t}{2(\psi \cdot T + G_0)} + \alpha \cdot \dot{\tau}_{oct}^{\beta} \cdot t^{(\beta+\kappa)} \cdot exp\left(\frac{-\lambda}{T}\right) \quad (13)$$

where $\dot{\tau}_{oct}$ is the octahedral shear stresses rate, ψ, G_0, α, β, κ, λ are empirical constants. Regression analysis on the test data using SPSS statistical software [15] these parameters are defined as: ψ = -54.04; G_0 = 25.82; α = 0.01, β = 2.018, κ = 0.129 and λ = 1559.24.

The elastic parameters E, G and ν can therefore be determined as:

$$E = -0.145T + 69.20 \quad GPa \quad (14)$$

$$G = -0.054T + 25.82 \quad GPa \quad (15)$$

$$\nu = (2\times10^{-4})T + 0.26 \quad (16)$$

The elastic and shear modulus linearly decrease with increasing temperature. The Poisson's ratio however tends to be independent of the temperature (Fig. 8).

6. STRAIN ENERGY DENSITY CRITERION

The strain energy density principle is applied to describe the salt strength and deformability

ASEAN++ 2013 Moving Forward
The 11th International Conference on Mining, Materials and Petroleum Engineering
The 7th International Conference on Earth Resources Technology
ASEAN Forum on Clean Coal Technology
November 11-13, 2013, Chiang Mai, Thailand

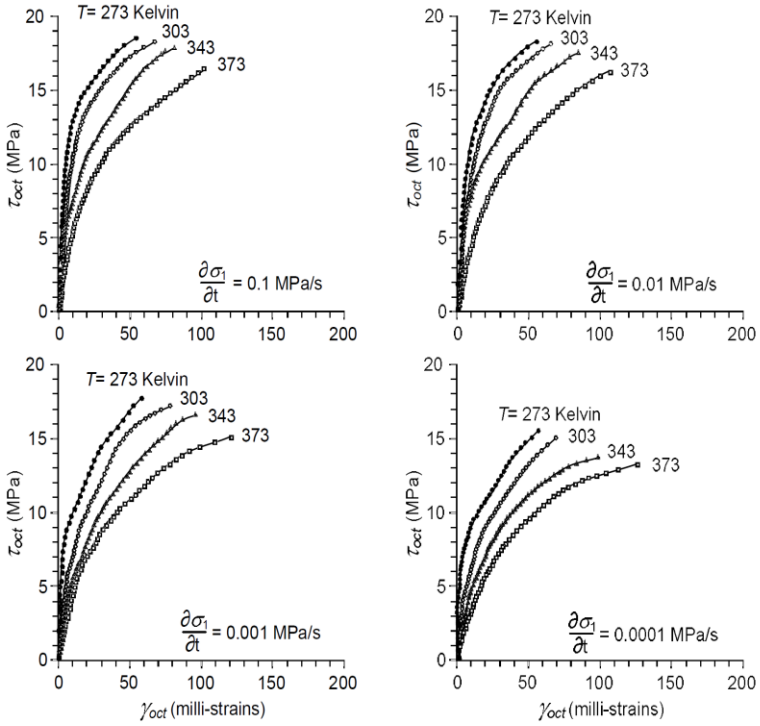

Fig. 6 Octahedral shear stress (τ_{oct}) as a function of octahedral shear strain (γ_{oct}) for various loading rates ($\partial\sigma_1/\partial t$) and temperatures ($T$).

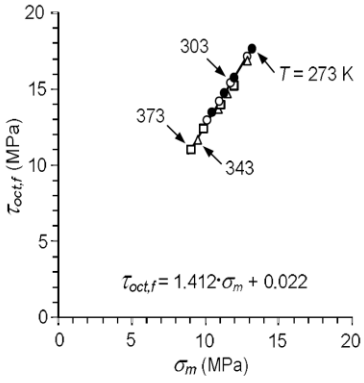

Fig. 7 Octahedral shear stress at failure ($\tau_{oct,f}$) of salt as a function of mean stress.

under different loading rates and temperatures. A similar approach has been used by Fuenkajorn et al. [5] to derive a loading rate-dependent strength for salt. The distortional strain energy at failure (W_d) can be calculated from the octahedral shear stresses and strains for each salt specimen using the following relations [13]:

$$W_d = (3/2)\cdot \tau_{oct,f}\cdot\gamma_{oct,f} \quad (17)$$

The distortion strain energy at failure (W_d) is presented as a function of the mean strain energy density at failure (W_m) which can be calculated from σ_m and ε_m as follows:

$$W_m = (3/2)\cdot\sigma_m\cdot\varepsilon_m \quad (18)$$

Fig. 9 shows a linear relation of W_d -W_m which can be represented by:

$$W_d = \omega\cdot W_m - \upsilon \quad (19)$$

The parameters ω and υ are empirical parameters. Tab. 2 gives W_d and W_m values calculated from the test results. The proposed criterion considers both stress and strain at failure, and hence isolating the effect of stress rate and temperature. If the salt temperature is known its strength can be determined from equation (19) regardless the loading rate.

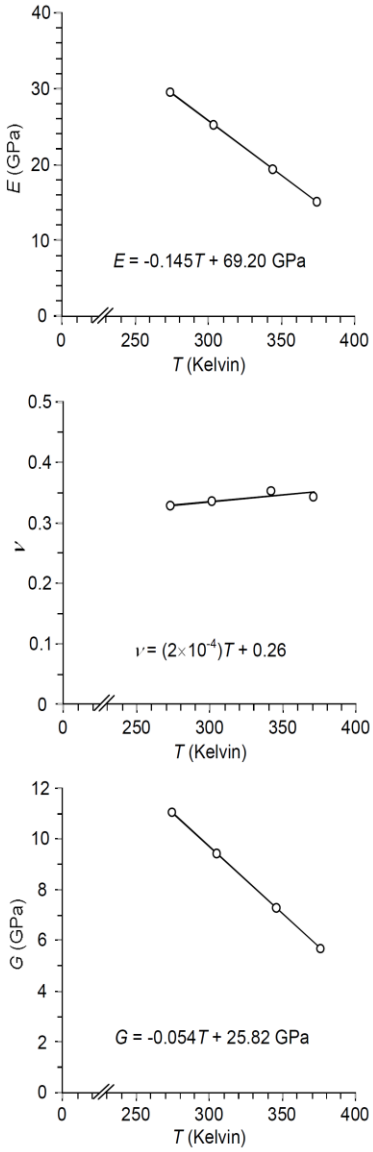

Fig. 8 Elastic modulus (E), Poisson's ratio (v) and Shear modulus (G) of salt as a function of temperature (T).

7. DISCUSSIONS AND CONCLUSIONS

The effect of loading rate and temperature on the compressive strength and deformability are determined for cylindrical salt specimens obtained from the Maha Sarakham formation. The applied axial stresses increases at constant rates of 0.0001, 0.001, 0.01 and 0.1 MPa/s.

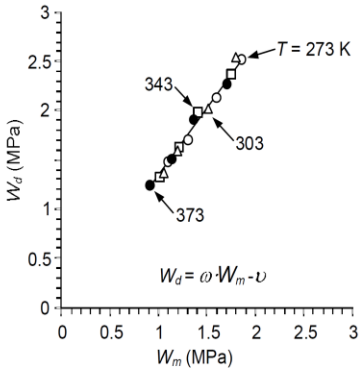

Fig. 9 Distortional strain energy at failure (W_d) as a function of mean strain energy (W_m).

The temperatures ranging of 273, 303, 343 and 373 Kelvin (0-100°C).

The testing is assumed to be under isothermal conditions (constant temperature with time during loading). The decrease of the salt strength as the temperature increases suggests that the applied thermal energy before the mechanical testing makes the salt weaker, and more plastic, failing at lower stress and higher strain with lower elastic and shear moduli. The failure stresses increase with the loading rates, these agree with the experimental results on rock salt performed by Fuenkajorn et al. [5] and Dubey and Gairola [16]. The proposed criterion can be used to determine the stability of rock salt around compressed-air or gas storage cavens during product injection (high temperature, low deviatoric stress) and retrieval (low temperature, high deviatoric stress).

ACKNOWLEDGMENTS

This study is funded by Suranaree University of Technology and by the Higher Education Promotion and National Research University of Thailand. Permission to publish this paper is gratefully acknowledged.

REFERENCES

[1] A.Kumar (1968), The effect of stress rate and temperature on the strength of basalt and granite, *Geophysic.*, 1968, Vol. 33, No. 3, pp. 501-510.

[2] J.C.Jaeger, and, N.G.W.Cook (1979), *Fundamentals of Rock Mechanics*, 3rd Edn, Chapman and Hall, London.

[3] N.D.Cristescu, and U.Hunsche (1998), *Time Effects in Rock Mechanics*, John Wiley & Sons, New York.

Tab. 2 Octahedral shear strength and strains and strain energy.

Average temperature (Kelvin)	Stress rate (MPa/s)	Octahedral Shear strength (MPa)	Octahedral shear strain (10^{-3})	Distortion strain energy density (MPa)	Mean strain energy density (MPa)
273	0.1	18.29	53.00	1.45	1.08
	0.01	16.47	54.58	1.35	1.00
	0.001	15.66	56.39	1.32	0.99
	0.0001	14.04	57.02	1.20	0.89
303	0.1	17.55	64.19	1.69	1.28
	0.01	16.29	65.17	1.59	1.18
	0.001	15.36	69.73	1.61	1.19
	0.0001	13.76	72.64	1.50	1.12
343	0.1	16.88	81.44	2.06	1.58
	0.01	15.80	83.80	1.99	1.46
	0.001	14.66	92.99	1.96	1.38
	0.0001	12.53	99.02	1.86	1.35
373	0.1	16.31	100.61	2.46	1.82
	0.01	14.85	112.49	2.51	1.83
	0.001	13.25	117.59	2.34	1.73
	0.0001	11.86	125.72	2.24	1.69

[4] M.Albertin, M.R.Julien, S.Servant, and D.E. Gill (1999), A rate-dependent model for the ductile behavior of salt rock, *Can. Geotech. J.*, 1999, Vol. 36, pp. 660-674.

[5] K.Fuenkajorn, T.Sriapai, and P.Samsri (2012), Effects of loading rate on strength and deformability of Maha Sarakham salt, *Eng Geol*., 2012, Vol. 135-136, pp. 10-23.

[6] W.G.Liang, Y.S.Zhao, S.G.Xu, and M.B.Dusseault (2011), Effect of strain rate on the mechanical properties of salt rock, *J. Min. Sci*., 2011, Vol.48, pp. 161-167.

[7] E.Z.Lajtai, E.J.Scott Duncan, and B.J.Carter (1991), The effect of strain rate on rock strength, *Rock Mech Rock Eng*., 1991, Vol. 24, pp. 99-109.

[8] M.Hamami (1999), Simulataneous effect of loading rate and confining pressure on the deviator evolution in rock salt, *Int. J. Rock Mech. Min. Sci*., 1999, Vol. 36, 827-831.

[9] T.Sriapai, C.Walsri, and K.Fuenkajorn (2012), Effect of temperature on compressive and tensile strength of salt, *Scienceasia*., 2012, Vol. 38, pp. 166-174.

[10] W.G.Liang, S.G.Xu, and Y.S.Zhao (2006), Experimental study of temperature effects on physical and mechanical characteristics of salt rock, *Rock Mech. Rock Engng*., 2006, Vol. 39, No. 5, pp. 469-482.

[11] V.I.Sheinin, and D.I.Blokhin (2012), Features of thermomechanical effects in rock salt samples under uniaxial compression, *J. Min. Sci*., 2012, Vol. 48, No. 1, pp. 39-45.

[12] M.E.Tabakh, C.Ultha-Aroon, and B.C.Schreiber (1999), Sedimentology of the Cretaceous Maha Sarakham evaporates in the Khorat plateau of northeastern Thailand, *Sedimentary Geol*., 1999, Vol. 123, pp. 31-62.

[13] J.C.Jaeger, N.G.W.Cook, And R.W.Zimmerman (2007), *Fundamentals of Rock Mechanics*, 4th Edn, Chapman and Hall, London.

[14] C.Yang, J.J.K.Daemen, and J.H.Yin (1999), Experimental investigation of creep behavior of salt rock, *Int. J. Rock Mech. Min. Sci*., 1999, Vol.36, pp. 233-242.

[15] L.Wendai (2000), Regression analysis, linear regression and probit regression In 13 chapters. *SPSS for Windows: statistical analysis*. Publishing House of Electronic Industry. Beijing.

[16] R.K.Dubey, and V.K.Gairola (2005), Influence of stress rate on rheology – An experimental study on rock salt of Simla Himalaya, India, *Geotech Geol Eng*., 2005, Vol. 23, pp. 757-772.

BIOGRAPHY

Miss. Suratwadee Sartkaew was born on February 26, 1990 in Mukdaharn province, Thailand. She received his Bachelor's Degree in Engineering (Geotechnology) from Suranaree University of Technology in 2011. For her post-graduate, he continued to study with a Master's degree in the Geological Engineering Program, Institute of Engineering, Suranaree university of Technology. During graduation, 2012-2013, she was a part time worker in position of research assistant at the Geomechanics Research Unit, Institute of Engineering, Suranaree University of Technology.